

Characteristics of chemically reacting compressible homogeneous turbulence

F. A. Jaberj,^{a)} D. Livescu, and C. K. Madnia^{b)}

Department of Mechanical and Aerospace Engineering, State University of New York, Buffalo, New York 14260

(Received 12 February 1999; accepted 10 January 2000)

Direct numerical simulations (DNS) are conducted to study the turbulence-chemical reaction interactions in homogeneous decaying compressible fluid flows. The reaction is of a single-step irreversible Arrhenius type. The results indicate that the heat of reaction has a noticeable influence on the solenoidal and the dilatational turbulent motions. The effect of reaction on the solenoidal velocity field is primarily due to variation of the molecular diffusivity coefficients with temperature and appears at small scales. However, the dilatational motions are affected more than the solenoidal motions and are intensified at all length scales. The decay rate of the turbulent kinetic energy is dependent on the molecular dissipation and the pressure-dilatation correlation. In isothermal reacting cases, the net contribution of the pressure-dilatation is small and the turbulent energy decays continuously due to viscous dissipation. In the exothermic reacting cases, the pressure-dilatation tends to increase the turbulent kinetic energy when the reaction is significant. Analysis of the flow structure indicates that the flow is dominated by strain in the reaction zones. Also, consistent with previous studies, the scalar gradient tends to align with the most compressive strain eigenvector and the vorticity vector tends to align with the intermediate strain eigenvector. The heat of reaction weakens this preferential alignment, primarily due to variation in molecular transport coefficients. The spatial and the compositional structure of the flame are also affected by the modification of the turbulence and the molecular coefficients. © 2000 American Institute of Physics.
[S1070-6631(00)00205-1]

I. INTRODUCTION

Modeling of turbulence-chemical reaction interactions continues to present a challenging task for engineers and scientists and remains an active area of research.¹⁻⁵ While there has been significant progress in understanding and modeling of turbulence and chemical reaction separately, much less is known about their coupled behavior.⁶ The nonlinear interactions between turbulence and chemical reaction occur over a wide range of time and length scales and involve many different quantities. Our lack of adequate understanding of these interactions imposes serious limitations on the modeling of chemically reactive turbulent flows. For example, the majority of existent turbulence closures which are used for reacting flow calculations are based on those developed for nonreacting flows. These closures are potentially limited and cannot account for important phenomena in turbulent combustion such as the extensive density and molecular property variations, significant dilatational turbulent motions, etc.

Previous numerical and experimental investigations involving flame-turbulence interactions primarily discuss the influence of the coherent structures on mixing and reaction in free shear flows⁷⁻¹³ (for recent reviews see Givi,¹

Dimotakis,¹⁴ Drummond and Givi,¹⁵ and Coats¹⁶). The results of these investigations indicate the importance of the large-scale as well as small-scale structures on the mixing and reaction. They also show that these structures are significantly affected by the exothermicity of the reaction and the flow compressibility. The effects of two-dimensional and three-dimensional turbulence on the structure of premixed and diffusion flames in shearless mixing layer are studied by Haworth and Poinso,¹⁷ Mahalingam *et al.*,¹⁸ and Boratav *et al.*¹⁹ via direct numerical simulation (DNS). Their results indicate that the structure of the flame is significantly altered by the turbulence.

Mixing and reaction in homogeneous turbulence have also been the subject of numerous investigations.²⁰⁻³³ In the majority of these investigations the flow is considered to be incompressible and the scalars are considered to be passive. Leonard and Hill,²⁵ and Nomura and Elgobashi,²⁸ study the structure of the reaction zone in homogeneous isotropic and shear incompressible turbulence via DNS. Their results show that the intense reaction rates occur over the regions where the concentration gradient is large and the gradients of the scalars tend to align with the direction of the most compressive eigenvector of the strain rate tensor. The effect of the compressibility on the turbulent mixing in homogeneous shear turbulence is studied by Blaisdell *et al.*³⁴ and Cai *et al.*³⁵ Their DNS results indicate that the dilatational convective velocity does not contribute noticeably to the mixing of the scalars.

^{a)}Present address: Department of Mechanical and Nuclear Engineering, Kansas State University, Manhattan, KS 66506-5205.

^{b)}Author to whom correspondence should be addressed; electronic mail: madnia@eng.buffalo.edu

The effects of the chemical heat release on the isotropic decaying and forced turbulence were recently studied by Balakrishnan *et al.*,³⁶ Jaberi and Madnia,³⁷ and Martin and Candler,³⁸ who consider different initial scalar conditions and chemical kinetics. Although these investigations reveal some interesting features of the turbulence-chemical reaction interactions in isotropic turbulence, more detailed studies have to be performed in order to fully understand the complex role portrayed by the combined influences of the turbulence and the chemical reaction in a compressible fluid medium. In this study, we use the data gathered from DNS of isotropic decaying turbulent reacting flows to further elucidate the interactions between turbulence and chemical reaction. The main objectives of this investigation are: (1) to analyze the flow and the flame structure, (2) to study the effects of the heat of reaction on different modes of energy, and (3) to examine the dynamical evolution of the vortical and the dilatational fluid motions and their correlation in the presence of chemical reaction in turbulent flows.

This paper is organized as follows. In Sec. II the governing equations are presented and the computational methodology for solving these equations is explained. The results pertaining to flame characteristics and the effect of heat of reaction on the flow structure, turbulent energy, and the solenoidal and dilatational turbulent motions are presented in Sec. III. A summary of important findings and conclusions is given in Sec. IV.

II. GOVERNING EQUATIONS AND COMPUTATIONAL METHODOLOGY

The primary independent transport variables in a compressible flow undergoing chemical reaction are the density ρ , the velocity components in x_i direction u_i , the specific energy e , the pressure p , the temperature T , and the mass fraction of species α , Y_α . The conservation equations governing these variables are expressed as

$$\frac{\partial \rho}{\partial t} + \frac{\partial}{\partial x_j} (\rho u_j) = 0, \quad (1)$$

$$\frac{\partial}{\partial t} (\rho u_i) + \frac{\partial}{\partial x_j} (\rho u_i u_j) = -\frac{\partial p}{\partial x_i} + \frac{1}{\text{Re}_o} \frac{\partial \Theta_{ij}}{\partial x_j}, \quad (2)$$

$$\begin{aligned} \frac{\partial}{\partial t} (\rho e) + \frac{\partial}{\partial x_j} (\rho u_j e) = & -\frac{\partial}{\partial x_j} (p u_j) \\ & + \frac{1}{(\gamma-1)M_o^2 \text{Re}_o \text{Pr}} \frac{\partial}{\partial x_j} \left(\mu \frac{\partial T}{\partial x_j} \right) \\ & + \frac{1}{\text{Re}_o} \frac{\partial}{\partial x_j} (u_i \Theta_{ij}) + Q, \end{aligned} \quad (3)$$

$$\frac{\partial}{\partial t} (\rho Y_\alpha) + \frac{\partial}{\partial x_j} (\rho u_j Y_\alpha) = \frac{1}{\text{Re}_o \text{Sc}} \frac{\partial}{\partial x_j} \left(\mu \frac{\partial Y_\alpha}{\partial x_j} \right) + w_\alpha, \quad (4)$$

where

$$\Theta_{ij} = 2\mu S_{ij} - \frac{2}{3}\mu\Delta\delta_{ij},$$

$S_{ij} = (1/2)(\partial u_i/\partial x_j + \partial u_j/\partial x_i)$ is the strain rate tensor, $\Delta = \partial u_k/\partial x_k$ is the dilatation, δ_{ij} is the Kronecker delta, and w_α and Q represent the chemical mass and heat source terms, respectively. The nondimensional viscosity, μ , is modeled as

$$\mu = T^n. \quad (5)$$

The specific energy is the summation of the specific internal (e_I) and kinetic (e_K) energies

$$e = e_I + e_K = \frac{p}{\rho(\gamma-1)} + \frac{1}{2}u_i u_i, \quad (6)$$

and thermodynamic variables are related through the equation of state

$$p = \frac{\rho T}{\gamma M_o^2}. \quad (7)$$

All variables in the above equations are normalized using reference length (l_o), velocity (u_o), temperature (T_o), and density (ρ_o) scales. Consequently, the important nondimensional parameters are the box Reynolds number, $\text{Re}_o = \rho_o u_o l_o / \mu_o$, the Prandtl number, $\text{Pr} = \mu_o c_p / \kappa_o$, the Schmidt number, $\text{Sc} = \mu_o / \rho_o \mathcal{D}_o$ and the reference Mach number, $M_o = u_o / \sqrt{\gamma R T_o}$ (R is the gas constant). The viscosity, μ_o , thermal diffusivity, κ_o , and mass diffusivity, \mathcal{D}_o , are assumed to be proportional to T_o^n , the specific heat at constant pressure, c_p , is constant and in all cases the Lewis number is unity with $\text{Pr} = \text{Sc} = 0.7$. Also, in all simulations $M_o = 0.6$ and $\gamma = 1.4$. The gas is assumed to be calorically perfect.

The chemistry is modeled with a single-step irreversible reaction of the type $A + rB \rightarrow (1+r)P$ ($r=1$ in this study) with an Arrhenius reaction rate,

$$\begin{aligned} w_A = w_B = & -\frac{1}{2}w_P = -\text{Da} \rho^2 Y_A Y_B \exp(-Ze/T), \\ Q = & \frac{\text{Ce}}{(\gamma-1)M_o^2} w_P. \end{aligned} \quad (8)$$

The mass fractions and the reaction rates of species A , B , P are represented by Y_A, Y_B, Y_P and w_A, w_B, w_P , respectively. The mass fraction of the mixture fraction, Z , is represented by Y_Z . All the species are assumed to be thermodynamically identical. The constant nondimensional quantities affecting the chemistry are the heat release parameter $\text{Ce} = -H^0/c_p T_o$, the Damköhler number $\text{Da} = K_f \rho_o l_o / u_o$, and the Zeldovich number $\text{Ze} = E_a / RT_o$, where $-H^0$ is the heat of reaction, K_f is the reaction rate parameter (assumed to be constant), and E_a is the activation energy.

Equations (1)–(4) are integrated using the Fourier pseudospectral method^{39,40} with triply periodic boundary conditions. The explicit second-order accurate Adams–Bashforth scheme is used to time advance the variables. All simulations are conducted within a box containing 128^3 collocation points. Aliasing errors are treated by truncating the Fourier values outside the shell with wave number $k_{\text{max}} = \sqrt{2}N/3$ (where N is the number of grid points in each direction). The velocity field is initialized as a random solenoidal, three-dimensional field with a zero mean and Gaussian spectral density function. The initial degree of compressibility is con-

TABLE I. The specifications of DNS cases.

Case #	Da	Ze	Ce	r_{CL} at $t=0$	n
1	2	0	0	0.008	0.7
2	2	0	0	0.124	0.7
3	200	8	3.168	0.008	0.7
4	200	8	3.168	0.008	0
5 ^a	200	8	3.168	0.008	0
6	200	8	1.584	0.008	0.7
7	300	8	1.584	0.008	0.7
8	3000	12	1.584	0.008	0.7
9	200	8	1.584	0.124	0.7

^aIn this special case the effect of chemical reaction on turbulence is removed.

trolled by varying the ratio of the energy residing in dilatational motions to the total energy.⁴¹ The initial pressure fluctuations are evaluated from a Poisson equation. The initial density field has unity mean value and no turbulent fluctuations and the initial values of the temperature are calculated from Eq. (7). The initial velocity field is allowed to decay to a ‘‘self-similar’’ state, corresponding to a fully developed turbulent flow, before scalar mixing and reaction begin. This corresponds to time $t=0$ on all the figures. The scalar A is specified in the physical domain in such a way as to yield a square wave in the x_2 -direction (slabs).³² The slabs are approximated by an error function distribution such that the scalar field varies smoothly in the range $0 < Y_A < 1$. The scalar values are constant in x_1-x_3 planes along the x_2 -direction. Cases with four scalar slabs are considered. The initial probability distribution function (PDF) of the scalar A is approximately composed of two delta functions centered at $Y_A=0,1$. The scalar B is perfectly anticorrelated with A and there are no products P in the domain at initial time.

III. RESULTS AND DISCUSSIONS

Direct numerical simulations of chemically reacting isotropic compressible decaying turbulence are performed. Table I provides the listing of the relevant information about each of the cases studied. The variable n in this table denotes the temperature exponent in Eq. (5). Cases 1 and 2 are the reference cases in which the reaction is constant rate with no heat release. The magnitude of r_{CL} (the ratio of the dilatational kinetic energy to the total kinetic energy as defined below) is different in these two cases. The initial value of r_{CL} is very small in case 1 but is significant in case 2. Cases 3–9 are considered to investigate the effects of heat release due to chemical reaction on the velocity, pressure, temperature, density, and scalar statistics. In cases 2 and 9 the initial flow compressibility is higher than the other cases listed in Table I. Case 4 is similar to case 3 but with constant molecular viscosity, conductivity, and diffusivity coefficients. This case is considered in order to isolate the effects of heat release on the molecular transport properties. Case 5 is also similar to case 3 but in this case in addition to Eqs. (1)–(4) an extra energy equation is solved in which the heat release term is neglected. The temperature obtained from this additional equation is used to calculate the pressure and the density. Therefore, in case 5 the effect of heat release on the

velocity field is eliminated. Case 5 is considered in order to isolate the effects of heat release on the mixing and reaction. The initial velocity field in case 1 and cases 3–8 are identical with Reynolds number based on Taylor microscale, $Re_\lambda = 50.1$ ($Re_\lambda = 50.7$ for cases 4 and 5 due to the difference in molecular viscosity) and $t_{eddy} = 1.8$ (t_{eddy} is the large scale eddy turnover time) and exhibits almost no contribution from the dilatational fluid motions. In cases 2 and 9, $Re_\lambda = 53.7$ and $t_{eddy} = 1.92$ at the initial time.

The temporal evolutions of the statistical quantities as extracted from DNS are of primary importance here. These statistics are obtained by volumetric averaging over all the collocation points. Two of the important statistical quantities are the mean and the variance of a variable α which are denoted by $\langle \alpha \rangle$ and $\sigma_\alpha = \langle (\alpha - \langle \alpha \rangle)^2 \rangle$, respectively. The variance of a vector is defined as the average of the variances of its three components. The three-dimensional (3D) spectral density function of the variable α ($\alpha \equiv v, T, p, \rho, A, Z$ etc.) is identified by $E_\alpha(k)$. The other important quantities are the local turbulent Mach number, M , and the enstrophy, Ω , which are defined as

$$M = \frac{\sqrt{u_i u_i}}{\sqrt{\gamma R T}}, \quad \Omega = \frac{1}{2} \omega_i \omega_i, \quad (9)$$

where ω_i denotes the vorticity vector. Of particular interest are the statistics of the solenoidal and the dilatational components of the velocity and the kinetic energy. To obtain these statistics, first the velocity (or the kinetic energy) is decomposed into the solenoidal and the dilatational parts according to the Weyl decomposition.^{41–43} Then the statistics are calculated for each component separately. In the discussion of the results below, the superscripts ‘‘s’’ and ‘‘d’’ denote the statistics that are calculated from the solenoidal and the dilatational velocity (or kinetic energy) components, respectively. For example, $E_v^s(k)$ and $E_v^d(k)$ denote the spectral density functions of the solenoidal and the dilatational velocities, respectively.

In the presentation of the results below, the ratios

$$r_{CS} = \frac{\langle \Delta^2 \rangle}{\langle \Omega \rangle + \langle \Delta^2 \rangle}, \quad r_{CL} = \frac{\sigma_v^d}{\sigma_v^s + \sigma_v^d}, \quad (10)$$

represent the flow compressibility at small (dissipation) and large (energy containing) scales, respectively.⁴⁴ The correlation coefficient between two variables a and b , $\zeta(a, b)$ is defined as

$$\zeta(a, b) \equiv \frac{\langle ab \rangle - \langle a \rangle \langle b \rangle}{[\langle a^2 \rangle - \langle a \rangle \langle a \rangle] [\langle b^2 \rangle - \langle b \rangle \langle b \rangle]}^{1/2}. \quad (11)$$

A. Flame characteristics

Characteristics of the flames considered in this study are identified via analysis of the flame structure. In turbulent reacting flows, the spatial and the compositional structure of the flame is dependent on the flow (turbulence) structure as well as the chemistry parameters. The flame structure is also dependent on the variations of the thermodynamic quantities since the reaction rate is dependent on these quantities. The

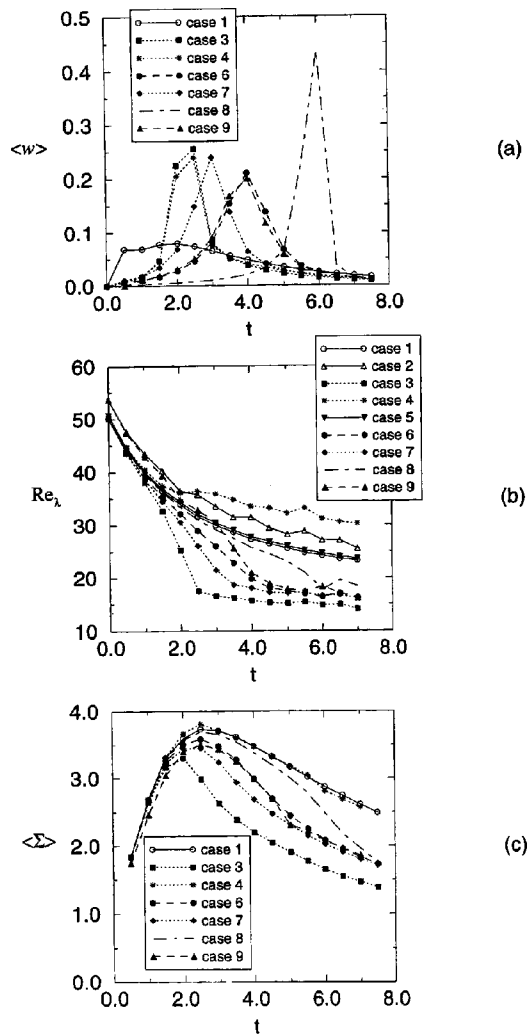


FIG. 1. Temporal variation of (a) the mean reaction rate, (b) Re_λ , and (c) the mean flame surface density.

heat of reaction, in turn, affects the turbulent motions and the thermodynamic variables, hence a two-way coupling exists.

In the assessment of the reaction, it is useful to study the reaction rate ($w \equiv -w_A$) and its components; the mixing term ($G = \rho^2 Y_A Y_B$) and the temperature-dependent term [$F = \exp(-Ze/T)$]. In the nonheat-releasing case 1, the reaction is solely dependent on G and its mean values as shown in Fig. 1(a), after reaching a peak at $t \approx 2$, decay continuously. However, in the heat-releasing cases, the reaction rate depends on both G and F and its maximum mean values occur at different times for different values of Da , Ze , and Ce . Expectedly, $\langle w \rangle$ peaks earlier as the values of Da and Ce increase or those of Ze decrease. The mean reaction rate is not, however, very much dependent on the initial flow compressibility as the results corresponding to cases 6 and 9 are very close. A comparison between the results in cases 3 and 4 also indicates that the variation in the magnitudes of the molecular transport coefficients has little effect on the temporal variation of $\langle w \rangle$. However, the Reynolds number is strongly affected by the variation in the molecular viscosity. This is illustrated in Fig. 1(b), where the time evolution of Re_λ is presented. The initial values of Re_λ vary between 50.1

(cases 1, 3, 6, 7, and 8) and 53.7 (cases 2 and 9). At $t = 2.5$, when the mean reaction rates for cases 3 and 4 reach their peak values, the values of Re_λ are between 17.5 (case 3) and 36.4 (case 4). The Reynolds number in case 4 is higher than that in case 1 due to the amplification of the dilatational fluid motions by the heat of reaction.

In modeling of turbulent reactive flows, the ‘‘flamelet assumption’’ is usually invoked. With this assumption, the reaction rate can be directly related to the mixture fraction through the flame surface density, Σ .^{5,45,46} In turbulent combustion, the flame surface density is a complex function of the flow and chemistry parameters. Following Pope,⁴⁷ we define the average flame surface density as

$$\begin{aligned} \langle \Sigma \rangle &= \langle |\nabla Y_Z| \delta[Y_Z - (Y_Z)_{st}] \rangle \\ &= \langle |\nabla Y_Z| |Y_Z = (Y_Z)_{st} \rangle \\ &\quad \times P(Y_Z = (Y_Z)_{st}), \end{aligned} \quad (12)$$

where δ is the Dirac-delta function, $\langle q | Y_Z = (Y_Z)_{st} \rangle$ is the expected value of the quantity q conditioned on $Y_Z = (Y_Z)_{st}$, and $P(Y_Z = (Y_Z)_{st})$ denotes the probability that $Y_Z = (Y_Z)_{st}$. Figure 1(c) shows the temporal evolution of the mean flame surface density for different cases. At early times, the values of $\langle \Sigma \rangle$ are relatively low and similar in all cases due to initial conditions. However, the flame surface density increases due to turbulent stretching/folding, and after peaking at $2 < t < 3$, decays due to scalar mixing and turbulence decay. A comparison among the results for cases 3 and 6 indicates that the late time values of $\langle \Sigma \rangle$ are lower for higher values of the heat release parameter. This is primarily due to variation of the molecular transport coefficients with temperature as the results in the heat-releasing case 4 with constant molecular coefficients are similar to those in nonheat-releasing case 1. This observation is further supported by the results obtained for case 7, which has a higher value of Da than case 6 and exhibits higher temperatures at earlier times. The small-scale scalar fluctuations are dependent on the magnitudes of the molecular transport coefficients and decay faster at higher temperatures, which results in lower values of Σ . However, it should be noted that the average $|\nabla Y_Z|$ conditioned on $(Y_Z)_{st}$ and probability of $(Y_Z)_{st}$, which appear in the flame surface density definition [Eq. (12)], are both affected by the heat release (not shown here). For case 4, these terms counteract each other and the net effect on the flame surface density is small.

A comparison between Figs. 1(a) and 1(c) clearly indicates that the temporal evolution of the mean flame surface density is very different from that of the mean reaction rate and the finite rate chemistry effects are important. Hewett and Madnia,⁴⁸ and Pierce and Moin,⁴⁹ also found that the finite rate chemistry effects become important under certain reacting flow conditions. To further explain the results in Fig. 1, the temporal variation of the volumetric averaged values of $\ln(G)$, $\ln(F)$, and $\ln(w)$ for case 3 are considered in Fig. 2. The results for other heat-releasing cases are qualitatively similar. Figure 2 shows that the evolution of the mean reaction rate is different than the mixing and the temperature-dependent terms. Expectedly, the mean values

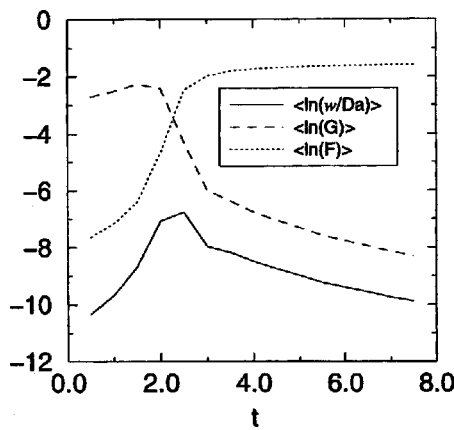


FIG. 2. Time variation of different terms in the reaction rate expression [Eq. (8)] for case 3.

of the temperature-dependent term, F , are very low at early times but increase significantly by the heat of reaction. The mixing term, G , exhibits behavior similar to that shown for the flame surface density in Fig. 1(c). The volumetric averaged values of this term increase at early times due to mixing of the reactants and decrease later due to consumption of the reactants. At $t=2.5$, when the mean reaction rate peaks (Fig. 1), the average values of F and G are comparable, showing the important contribution of both mixing and temperature to the reaction rate.

In order to further identify the role of reaction in the flow field, three regions are defined based on the mean values of w , F , and G at $t=2.5$. Table II presents the percentage of the computational grid points corresponding to these three regions,

- (i) Region I: $w > \langle w \rangle_{t=2.5}$,
- (ii) Region II: $w < \langle w \rangle_{t=2.5}, G > \langle G \rangle_{t=2.5}, F < \langle F \rangle_{t=2.5}$,
- (iii) Region III: $w < \langle w \rangle_{t=2.5}, G < \langle G \rangle_{t=2.5}, F > \langle F \rangle_{t=2.5}$,

at different times. The regions I, II, and III may be associated with the ‘‘reaction region,’’ the ‘‘mixing region,’’ and the ‘‘hot-product region,’’ respectively. The results in Table II are consistent with the results shown in Fig. 6 below, and indicate that at $t=1$ a significant portion of the domain consists of region II. At this time the reaction rate and the temperature are relatively low and regions I and III have a negligible contribution. At $t=2.5$, when the mean reaction rate is significant, most of the field is composed of region I. At later times ($t=4$), when the mean reaction rate is small, the mixing and the reaction occur rarely and the total volume occupied by regions I and II is less than 1% of the computational domain.

TABLE II. Percentage of the domain filled with regions I, II, and III.

	Region I	Region II	Region III
$t=1$	0%	75%	0%
$t=2.5$	40%	15%	26%
$t=4$	0.5%	0%	93.5%

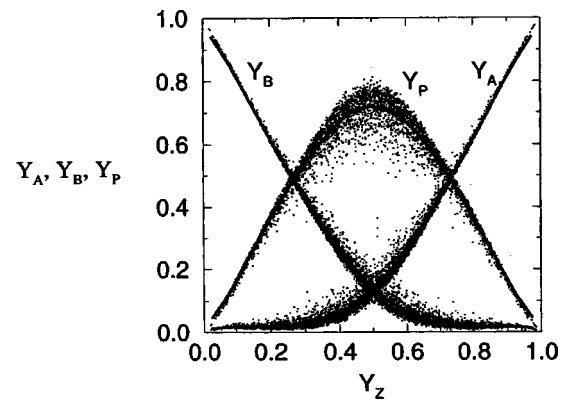


FIG. 3. Scatter plots of the reactants and product mass fractions in mixture fraction (Z) space for case 3 at $t=2.5$ (sample size 4096 points). The solid lines represent the conditional means and are calculated based on all grid points (128^3).

The results in Figs. 1 and 2 and Table II show the average behavior of the reaction at different times and do not provide information about the flame structure. The flame structure can be studied by examination of the reactive species in mixture fraction (compositional) space. Figure 3 shows the scatter plots of the reactants and the product mass fractions in mixture fraction space for case 3. These scatter plots are similar to those of a typical flame with finite rate chemistry effects.

The scatter plot of the reaction rate in mixture fraction space for case 3 at $t=2.5$ is shown in Fig. 4(a). This figure indicates that the conditional mean value of the reaction rate is the highest at the stoichiometric surface ($Y_Z=0.5$), similar to that observed in Fig. 3 for product mass fraction. However, the variation of the reaction rate in mixture fraction space is different than that of the product mass fraction. To explain this behavior, the scatter plots of G and F parts of the reaction rate are shown in Figs. 4(b) and 4(c). The F term is only a function of temperature and behaves similar to Y_P . The behavior of the G term is more complex. This term depends on the density and the product of the reactants’ mass fractions, and as shown in Fig. 4(c) attains relatively low values near the stoichiometric surface, mainly due to low values of the density [Fig. 4(d)]. At later times ($t>2.5$), as shown in Fig. 2, the F term is larger than the G term and the scatter plots of w exhibit behavior similar to F and Y_P . It should be noted that, due to homogeneity of the flow, the reaction in this study occurs through a constant volume process. Therefore, the mean density is constant but the mean pressure and temperature increase continuously and similarly. Within the reaction zone, the density decreases due to volumetric flow expansion and is lower than unity. Outside this zone the density is higher than unity, as shown in Fig. 4(d).

It is shown above that in exothermic reacting cases the mixing term and the temperature-dependent term both contribute significantly to the reaction. However, the mean values of these terms evolve very differently. This raises the question of how the local values of these terms are correlated with each other and with the reaction rate. To answer this question, the temporal variation of the correlation coefficient

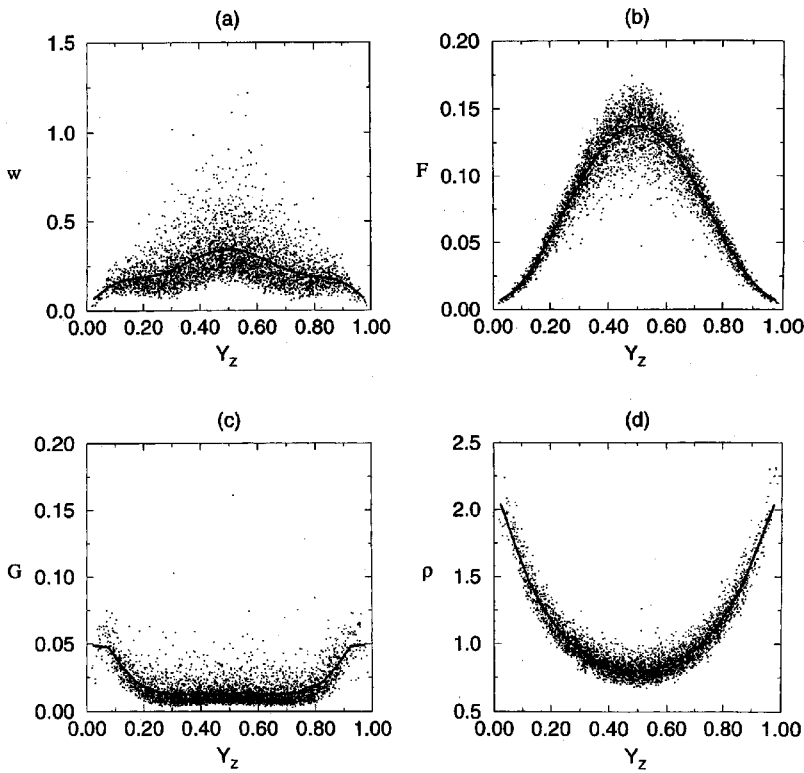


FIG. 4. Scatter plots of (a) w , (b) F , (c) G , and (d) ρ , in mixture fraction space for case 3 at $t=2.5$ (sample size 4096 points). The solid lines represent the conditional means and are calculated based on all grid points (128^3).

between G and w and that between G and F for case 3 are shown in Fig. 5. The results for other heat-releasing cases are qualitatively similar and are not shown. It is evident that the G term is not well correlated with the reaction rate when the rate of reaction is significant. This lack of correlation between G and w has a significant influence on the spatial flame structure and is explained below.

Figure 6 shows the joint PDF of G and F and the joint PDF of G and w at several different times. At early times ($t=1$), as indicated in Table II, in most of the domain the reaction is insignificant and is confined to the mixing zones. This explains the strong correlation between w and G at early times as observed in Fig. 5. Also, at early times the temperature increases only in the regions where the reaction takes place and there is a good correlation between F and G (Fig. 5). The joint PDF plot in Fig. 6(b) confirms that F and G are indeed well correlated. At $t=2.5$, when the mean reaction

rate is high, the field is primarily composed of zones with high temperature (hot-product region, 26% of the total number of points, and reaction region with $G < \langle G \rangle$, 22% of the field) and of zones with mixed reactants (mixing region, 15% of the field, and low-temperature reaction region with $F < \langle F \rangle$, 10%). In the zones with mixed reactants the temperature has not yet increased significantly, so $G > \langle G \rangle$ and $F < \langle F \rangle$ in these zones [Fig. 6(d)]. In the high-temperature zones, $G < \langle G \rangle$ and $F > \langle F \rangle$. These results are consistent with Fig. 5, where it is shown that F and G are negatively correlated at $t=2.5$. Although there are regions in the flow with very high values of G and w , in most of the domain the values of G and w are moderate to low [Fig. 6(c)]. The points in the domain are relatively evenly distributed among the four regions defined by the lines $G = \langle G \rangle$ and $w = \langle w \rangle$ on Fig. 6(c). As a result, the correlation between G and the reaction rate is very low at $t=2.5$ (Fig. 5). At later times, most of the reactants have already burnt and, as shown in Table II, the field is occupied almost entirely by hot products. At these times, F is almost evenly distributed around its mean [Fig. 6(f)] and the correlation between F and G is low. At elevated temperatures, the exponential term has small spatial variation and F is nearly constant. Therefore, the reaction rate as illustrated in Figs. 5 and 6(e) is highly correlated with G . Figure 6(e) also shows that at $t=4$ there are still some rare regions in which mixing and reaction are both significant.

So far, we have only discussed the influence of various parameters on the reaction. In the following sections the effects of reaction on turbulence are studied. In particular we will show how the turbulence structure, the turbulent energy, the vorticity field, and the dilatation field are affected by the reaction. The influence of the reaction on the thermodynamic

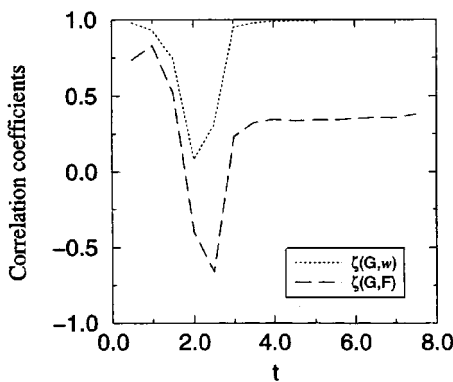


FIG. 5. Temporal variation of the correlation coefficient between G and F and G and w , in case 3.

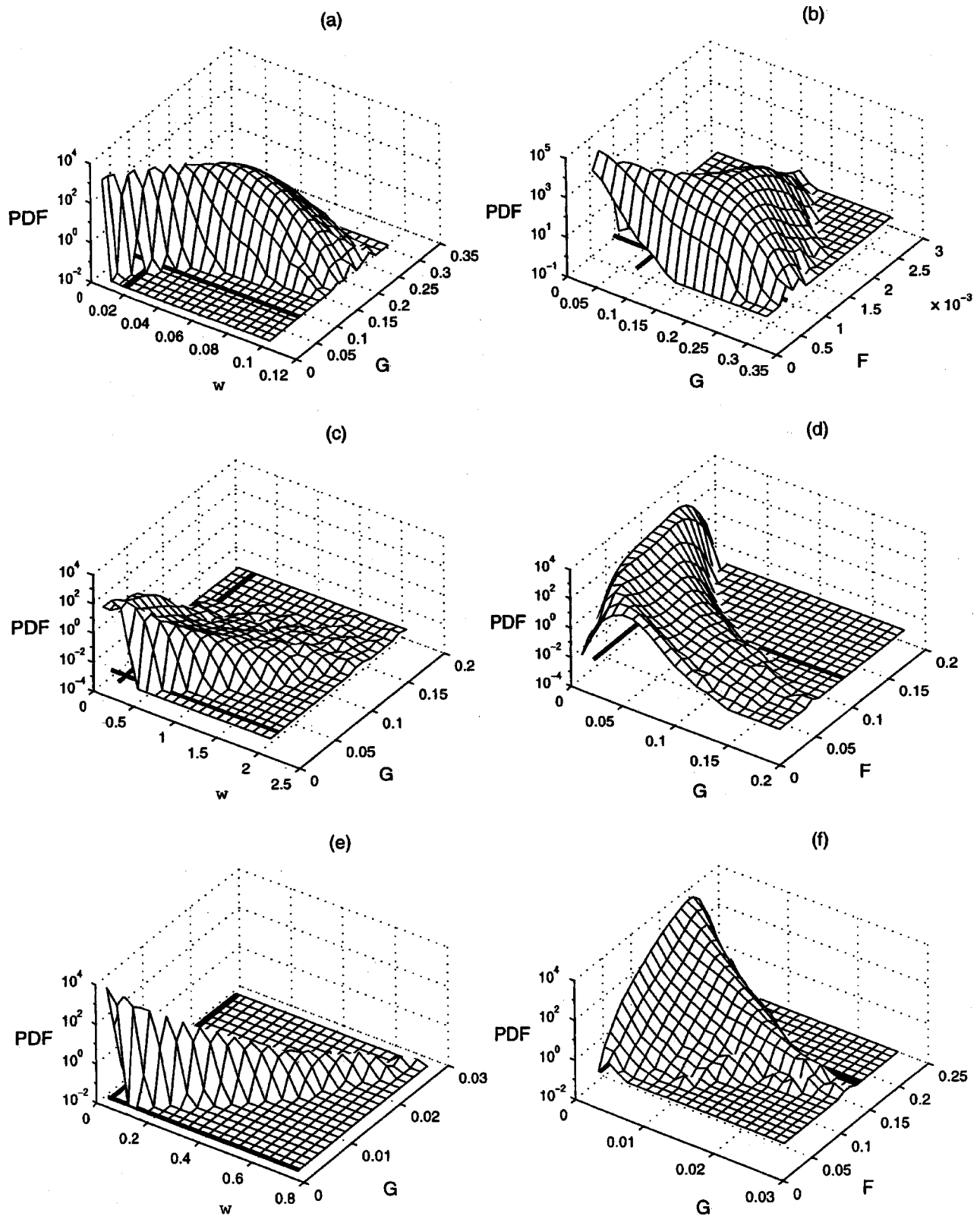


FIG. 6. Joint PDF of (a) w and G at $t=1$, (b) G and F at $t=1$, (c) w and G at $t=2.5$, (d) G and F at $t=2.5$, (e) w and G at $t=4$, (f) G and F at $t=4$, for case 3. The thick lines represent the average values which are respectively: $\langle G \rangle_{t=1.0}=0.087$, $\langle w \rangle_{t=1.0}=0.017$, $\langle F \rangle_{t=1.0}=0.0008$, $\langle G \rangle_{t=2.5}=0.017$, $\langle w \rangle_{t=2.5}=0.255$, $\langle F \rangle_{t=2.5}=0.096$, $\langle G \rangle_{t=4.0}=0.001$, $\langle w \rangle_{t=4.0}=0.038$, $\langle F \rangle_{t=4.0}=0.16$.

variables is also studied. The results are consistent with those of Balakrishnan *et al.*,³⁶ Jaber and Madnia,³⁷ and Martin and Candler,³⁸ and indicate that the fluctuations of the temperature and pressure increase significantly by the heat of reac-

tion. Although the value of density is minimum at the stoichiometric surface [Fig. 4(d)], its fluctuations increase as the rate of heat release increases. The rate of heat release is dependent on the density, temperature, and reactants' mass

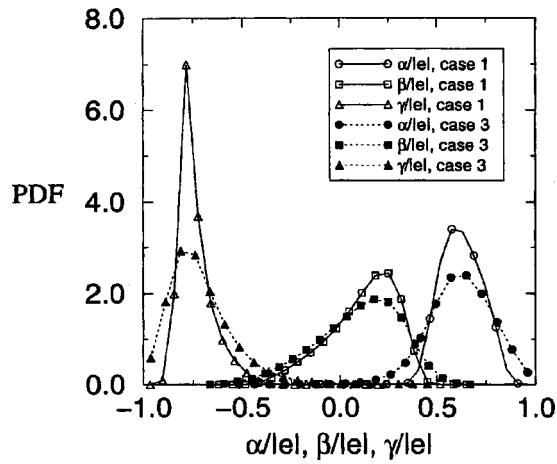


FIG. 7. PDF of the normalized eigenvalues of the strain rate tensor for cases 1 and 3 at $t=2.5$.

fractions and varies significantly throughout the flow field. The nonuniform generation of heat results in the enhancement of the fluctuations of thermodynamic variables. The variations in temperature and density in turn result in modification of the reaction rate.

B. Flow structure

The heat of reaction has a noticeable influence on turbulence structures. This is partially demonstrated in this section via analysis of the strain rate tensor [$S_{ij}=1/2(\partial u_i/\partial x_j + \partial u_j/\partial x_i)$] and alignment of its eigenvectors with the vorticity and scalar gradient vectors. The eigenvalues of the strain tensor or the principal strain rates are termed conventionally as α, β, γ , with $\alpha > \beta > \gamma$. The PDFs of the eigenvalues of the strain rate normalized by the magnitude of total strain ($|e|=(\alpha^2 + \beta^2 + \gamma^2)^{1/2}$) for cases 1 and 3 at $t=2.5$ are shown in Fig. 7. It is observed that although the shape of the PDFs is not substantially affected, the heat of reaction increases the variances of all eigenvalues. In agreement with the previous observations,^{22,25,50} the values of β are shown to be mostly positive. Also, due to homogeneity in all cases considered in this study $\langle \alpha + \beta + \gamma \rangle \approx 0$. The reaction has also a noticeable influence on the average values of the principal strain rates. This is observed in Fig. 8, where it is shown that the magnitudes of $\langle \alpha \rangle$, $\langle \beta \rangle$, and $\langle \gamma \rangle$ decay faster

as the heat release increases. The heat of reaction increases the magnitudes of the molecular transport coefficients and results in faster decay of the turbulence and the strain eigenvalues.

To further examine the effect of reaction on the flow structures, the PDFs of the cosines of angles between the vorticity and the principal strain directions for cases 1 and 3 are plotted in Fig. 9(a). The angles between the vorticity vector and α -, β -, and γ -eigenvectors are denoted by ζ_1, ζ_2 , and ζ_3 , respectively. Direct numerical simulations of incompressible nonreacting turbulent flows suggest a preferential alignment among the strain eigenvectors, the vorticity vector, and the scalar gradient vector.^{22,28,51-55} This preferential alignment is due mainly to local effects associated with the structure and dynamics of vorticity vector and strain rate tensor,^{26,56-58} although the formation of distinct spatial structures can also affect the alignment.⁵⁸ It has been found that the vorticity vector tends to align with the direction of the intermediate (β) strain eigenvector and the scalar gradient vector tends to align with the direction of the most compressive (γ) strain eigenvector. The PDF plots in Fig. 9(a) also show that the vorticity vector tends to be parallel to the β -eigenvector and perpendicular to the γ -eigenvector in both heat releasing and non-heat-releasing cases. The effect of heat of reaction is to decrease the alignment of the vorticity vector with the β -eigenvector and to increase the alignment with the α -eigenvector. It is interesting to note that these results, as obtained for a homogeneous (constant volume) flow, agree qualitatively with the results of Nomura and Elgobashi⁵⁹ obtained for an inhomogeneous flow with constant molecular coefficients and infinitely fast chemistry. The PDFs obtained for case 4 (not shown here) are similar to those shown in Fig. 9(a) for case 1. This suggests that the modification of the alignment of the vorticity vector and strain eigenvectors is primarily due to variation of the molecular transport coefficients with temperature.

A more detailed analysis of our results indicates that the alignment between the vorticity vector and the strain eigenvectors is more significantly affected by the reaction in the “reaction zones,” where the values of the mixture fraction are close to the stoichiometric values. Our results are also consistent with those obtained by Boratav *et al.*,¹⁹ and indicate that in the reaction zones the flow is dominated by strain

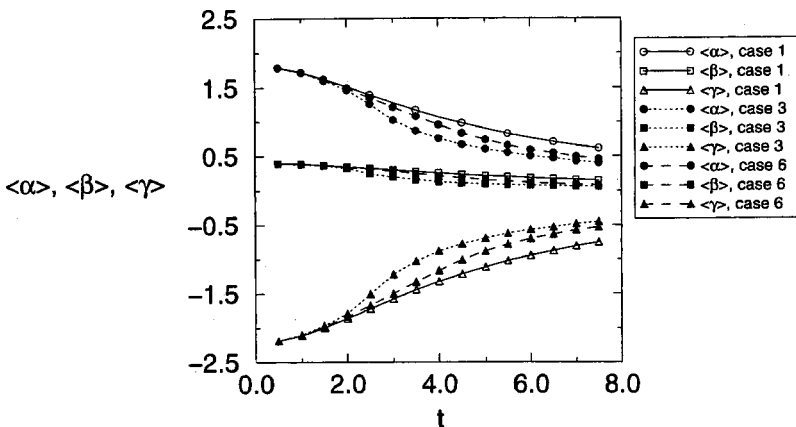


FIG. 8. Temporal variation of the mean values of the strain rate eigenvalues.

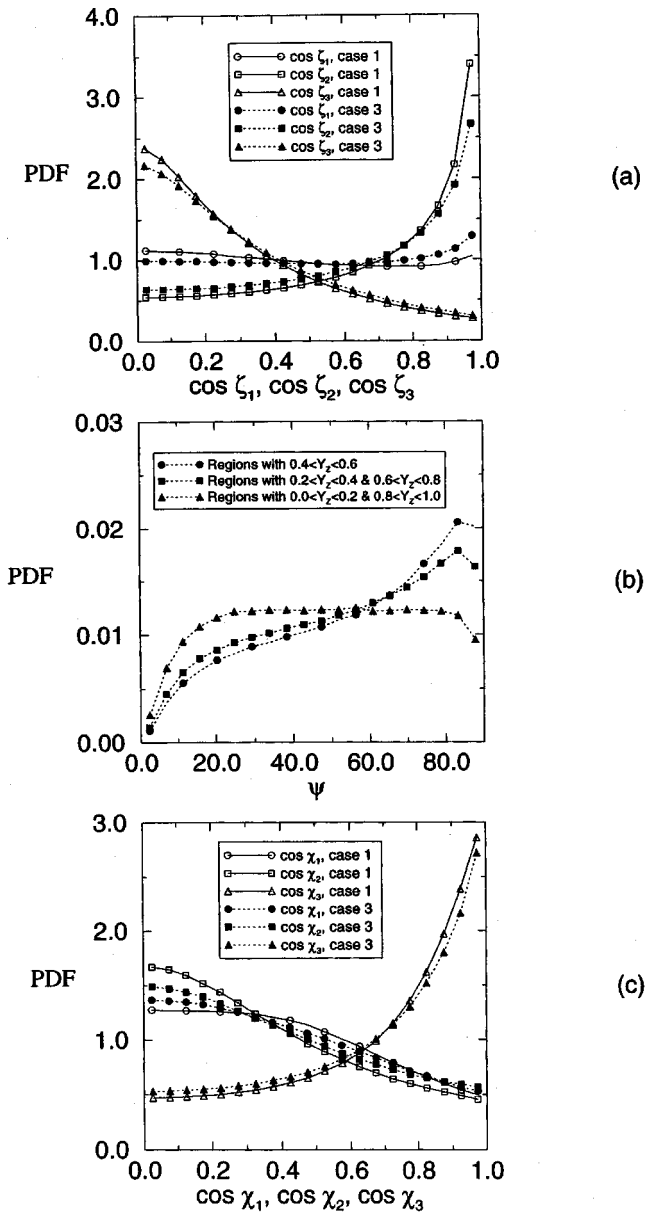


FIG. 9. (a) PDFs of the cosine of the angles between the eigenvectors of the strain rate tensor and the vorticity vector at $t=2.5$, (b) PDFs of Ψ for case 3 at $t=2.5$, (c) PDF of the cosine of the angles between the eigenvectors of the strain rate tensor and the gradient of Y_Z .

rather than rotation. This is demonstrated in Fig. 9(b), where the PDFs of Ψ , sampled over three different ranges of Y_Z , are considered. The strain-ensrophy angle, Ψ , is defined as¹⁹

$$\Psi = \tan^{-1} \frac{S_{ij} S_{ij}}{R_{ij} R_{ij}},$$

where R_{ij} is the rotation tensor. By definition, large values of Ψ ($\geq 45^\circ$) correspond to the strain-dominated flow regions and small values of Ψ ($\leq 45^\circ$) correspond to the enstrophy-dominated regions. Figure 9(b) shows that in the reaction zones the flow is dominated by the strain and the vortical fluid motions play a lesser role. The conditional expected values of the enstrophy, conditioned on Y_Z , for the heat-releasing cases (not shown) are also consistent with Fig. 9(b)

and indicate that the lowest and highest values are obtained inside and outside the reaction zone, respectively.

Figure 9(c) shows the PDF of the cosine of the angle between the scalar gradient vector and the principal strain directions for cases 1 and 3 at $t=2.5$. The angles with α -, β -, and γ -eigenvectors are denoted by χ_1 , χ_2 , and χ_3 , respectively. In both cases, the scalar gradient tends to align with the most compressive principal direction of the strain rate tensor as observed previously.^{50,54,55} Our results (not shown) also indicate that in both heat-releasing and non-heat-releasing cases the scalar gradient tends to be mainly normal to the vorticity vector. The heat of reaction has little effect on the alignment of strain eigenvectors and the scalar gradient. The main effect of the reaction is that the PDFs of $\cos(\chi_1)$ and $\cos(\chi_2)$ are closer to each other in heat-releasing cases. A comparison with the results obtained for case 4 (not shown here) again suggests that the change in the alignment among strain eigenvectors and the scalar gradient is due to variation of the molecular transport coefficients with temperature.

C. Turbulent energy

In this section the effects of reaction on the turbulent kinetic energy and the energy transfer among different components of the kinetic energy and the internal energy are studied. The effect of heat of reaction on the mean turbulent kinetic energy is shown in Fig. 10(a). This figure shows that the reaction has little effect on the decay of the turbulent kinetic energy (compare cases 1 and 3). The reason that the decay rate of the kinetic energy is not significantly affected by the reaction is explained by considering the effects of reaction on different components of the kinetic energy. The turbulent kinetic energy is composed of the rotational (solenoidal) and the compressive (dilatational) components. In the absence of heat release, the values of the dilatational and the solenoidal turbulent kinetic energies decay slowly due to viscous dissipation. However, both components of the kinetic energy are affected by the reaction [Figs. 10(b) and 10(c)]. The results in Fig. 10(b) indicate that the solenoidal kinetic energy decays faster due to the heat of reaction (compare cases 1 and 3). This is primarily due to an increase in the magnitudes of the molecular transport coefficients and turbulent kinetic energy dissipation with temperature. The influence of the heat of reaction on the dilatational component of the kinetic energy is different than that on the solenoidal component. Figure 10(c) shows that the mean values of the dilatational kinetic energy increase significantly due to heat release, despite the fact that the magnitude of turbulent Mach number decreases by the reaction. Figure 10(c) also shows that the generated dilatational motions remain significant, long after the reaction is completed. The results corresponding to cases 3 and 4 indicate that the variation in the magnitudes of the molecular diffusivity coefficients does not have a significant effect on the evolution of dilatational kinetic energy.

Figures 10(b) and 10(c), therefore, explain the results shown in Fig. 10(a). The solenoidal kinetic energy is affected

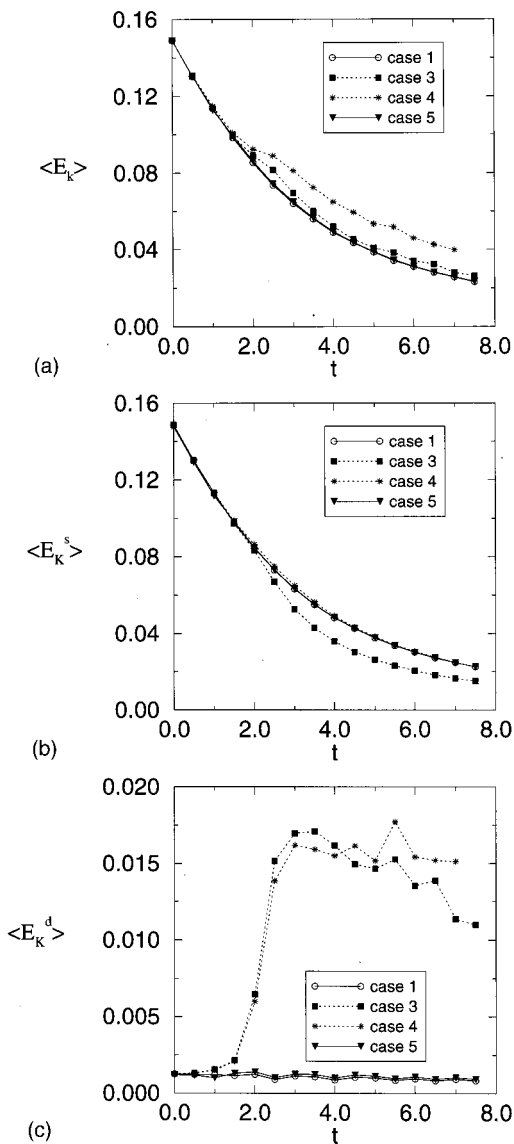


FIG. 10. Temporal variations of (a) the turbulent kinetic energy, (b) the solenoidal component of the turbulent kinetic energy, and (c) the dilatational component of the turbulent kinetic energy.

by the reaction, primarily due to variation in molecular coefficients. In contrast, the reaction increases the values of the mean dilatational kinetic energy. The net effect on kinetic energy would be the summation of the effects on its solenoidal and dilatational components. A comparison between cases 1 and 3 in Fig. 10(a) indicates that the reaction slightly modifies the decay rate of the mean kinetic energy. In case 4, the molecular viscosity is constant and the mean values of the solenoidal energy are not significantly affected by the reaction. However, the dilatational energy increases substantially by the reaction. Consequently, the mean values of the kinetic energy in case 4 are significantly higher than those in case 1. From the results presented in Fig. 10 it can be concluded that the volumetric flow expansion, on average, does not have a significant effect on the solenoidal turbulent motions.

Figure 10 shows that the heat of reaction has a significant influence on the turbulent energy. However, this figure

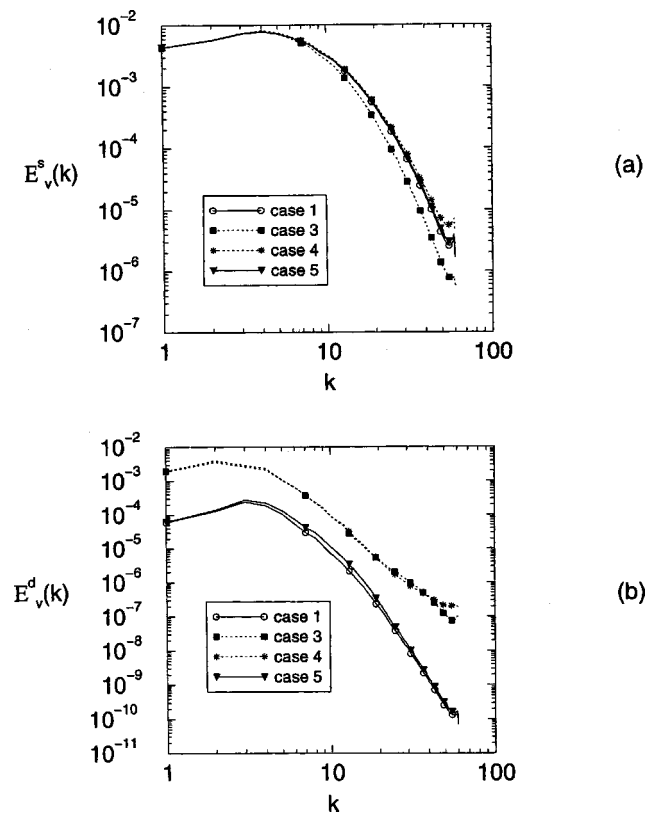


FIG. 11. Three-dimensional spectral density functions of (a) the solenoidal velocity, (b) the dilatational velocity, at $t=3$.

cannot reveal how different turbulent scales are affected by the reaction. The interaction between turbulence and chemical reaction occurs over a variety of different length scales and it is important, from both physical understanding and a modeling point of view, to assess the influence of reaction on different flow scales. To address this issue, the 3D spectral density function of the solenoidal and the dilatational velocity for several different cases are considered in Fig. 11. It is shown in Fig. 11(a) that the large-scale solenoidal velocity field is not noticeably altered by the reaction and is similar in cases with constant and temperature-dependent diffusivity coefficients. However, the small-scale solenoidal turbulent motions are dependent on the magnitudes of the molecular transport coefficients and are affected by the heat of reaction. As compared to case 1, the magnitudes of the molecular coefficients are higher and the small scales decay faster in case 3. The small-scale values of the solenoidal energy in case 4 are slightly higher than those in case 1, since in case 4 a net energy is transferred from the internal energy to the kinetic energy by the pressure-dilatation correlations. This is explained in more detail below, where the transport equations for internal and kinetic energies are considered.

In contrast to the solenoidal velocity spectrum, the dilatational velocity spectrum is significantly affected by the heat release at all length scales. This is demonstrated in Fig. 11(b), where it is shown that the large- and the small-scale dilatational energy in cases 3 and 4 is significantly higher than that in cases 1 and 5. Nevertheless, the spectra in cases 3 and 4 are very close to each other. This suggests that the

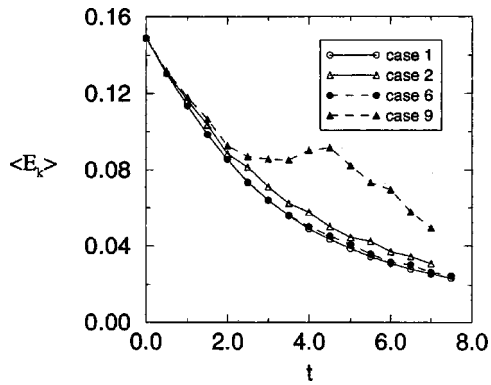


FIG. 12. Temporal variation of the mean kinetic energy for different cases.

dilatational velocity field is modified by the heat of reaction, primarily due to volumetric flow expansion/contraction, and the variation in molecular transport coefficients has little effect.

The effect of the initial flow compressibility on the decay of the mean turbulent kinetic energy for both non-heat-releasing and heat-releasing cases is shown in Fig. 12. In non-heat-releasing cases, the kinetic energy decays more slowly as the flow compressibility increases. The results in Fig. 12 are also consistent with those in Fig. 10(a) and indicate that the decay of the turbulent kinetic energy is not significantly affected by the heat of reaction when the initial flow compressibility is small (compare cases 1 and 6). However, the reaction changes the mean kinetic energy, when the initial flow compressibility is significant (compare cases 2 and 9). An examination of different components of the turbulent kinetic energy for cases 2 and 9 indicates that while the dilatational component increases by the reaction the solenoidal component decreases. Our results (not shown) also indicate that the effects of reaction on the dilatational turbulent energy and the thermodynamic variables are dependent on the initial flow compressibility. In the cases in which the initial variations in temperature and density are more significant, the variation in the reaction rate would also be more significant and the thermodynamic variables as well as the dilatational turbulent motions are affected more by the heat of reaction.

1. Energy transfer

To examine the effects of the reaction on the energy transfer between the internal ($E_I = \rho e_I$) and the kinetic ($E_K = \rho e_K$) energies, the transport equations for $\langle E_I \rangle$ and $\langle E_K \rangle$ are considered,

$$\frac{d}{dt} \langle E_I \rangle = -\langle PD \rangle - \langle VD \rangle + \langle HR \rangle, \quad (13)$$

$$\frac{d}{dt} \langle E_K \rangle = \langle PD \rangle + \langle VD \rangle, \quad (14)$$

where

$$\langle PD \rangle \equiv \left\langle p \frac{\partial u_j}{\partial x_j} \right\rangle,$$

$$\langle VD \rangle \equiv \left\langle \Theta_{ij} \frac{\partial u_i}{\partial x_j} \right\rangle,$$

$$\langle HR \rangle \equiv \frac{Ce}{(\gamma - 1)M_o^2} \langle w_P \rangle,$$

are the ‘‘pressure-dilatation,’’ the ‘‘viscous-dissipation,’’ and the ‘‘heat-release’’ terms, respectively.³⁷ Examination of Eqs. (13) and (14) indicates that the heat of the reaction is directly transferred to the internal energy and the mean kinetic energy may only be modified indirectly through the variations in the pressure-dilatation and viscous-dissipation terms. The total energy ($E_T = E_I + E_K$) is only affected by the heat of reaction and is constant in non-heat-releasing cases. In the heat-releasing cases considered here, the values of the internal energy are much larger than those of the kinetic energy and monotonically increase by the heat of reaction.

The rate of variation of the mean kinetic and internal energies, as discussed above, are dependent on the pressure-dilatation, viscous-dissipation, and heat-release terms. Detailed examination of each of these terms helps us explain the results in Figs. 10–12. In the heat-releasing cases considered in this study, the magnitudes of the heat-release term are much larger than those of the pressure-dilatation and viscous-dissipation terms and the internal energy varies primarily due to this term. The heat of reaction does not have any direct influence on the kinetic energy. However, the rate of change of the kinetic energy is controlled by the pressure-dilatation and the viscous-dissipation terms. Both of these terms as shown in Fig. 13 are affected by the heat of reaction. In the non-heat-releasing case 1, the values of the pressure dilatation oscillate around zero, indicating that the energy is alternatively transferred between the internal and the kinetic energies via this term. In this case, the pressure-dilatation term is relatively small as the flow is nearly incompressible. However, consistent with the results of Balakrishnan *et al.*,³⁶ Jaber and Madnia,³⁷ and Martin and Candler,³⁸ the amplitude of the oscillation of the pressure-dilatation term is significantly increased by the heat of reaction. Figure 13(a) shows that the values of this term in cases 3 and 4 are an order of magnitude larger than those in case 1. Comparisons of the results for cases 1 and 5 and cases 3 and 4 indicate that the variation in molecular coefficients has little effect on the evolution of the pressure dilatation.

Temporal variations of the viscous-dissipation term for different cases are shown in Fig. 13(b). In non-heat-releasing case 1, this term has the dominant effect and decreases (increases) the kinetic (internal) energy. With the decay of turbulence, the gradients of the velocity and the magnitudes of the viscous-dissipation term decrease. Nevertheless, the magnitudes of this term in heat-releasing case 3 are considerably larger than those in non-heat-releasing case 1. This is due to modification of the molecular coefficients and the small-scale turbulence by the heat of reaction. The most significant difference between the results in cases 1 and 3 occurs at $1.5 < t < 3$, when the reaction is very important. A comparison among the results in cases 1, 3, and 4 indicates that the magnitudes of the viscous-dissipation term increase prima-

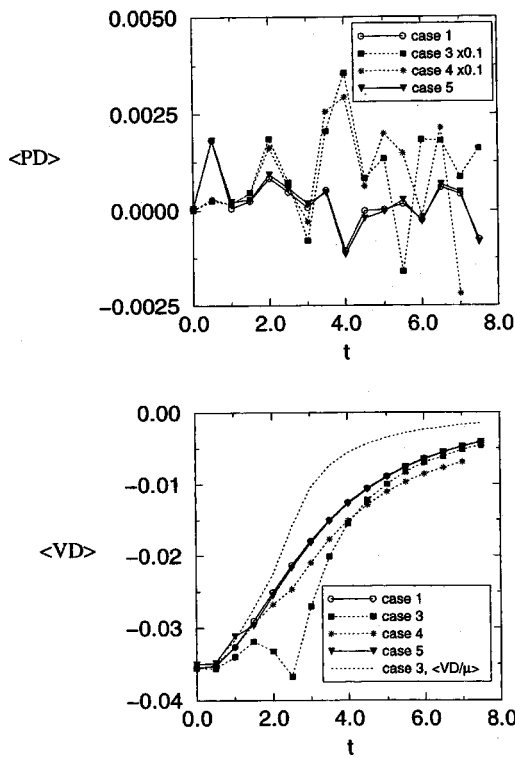


FIG. 13. Temporal variation of (a) the pressure dilatation $\langle PD \rangle$, and (b) the viscous dissipation $\langle VD \rangle$.

rily due to increase in the molecular coefficients. The volumetric expansion/contraction of the fluid elements also slightly increases the magnitudes of the viscous-dissipation term (compare cases 1 and 4). Interestingly, the long time values of $\langle VD \rangle$ in case 3 are smaller than those in case 4, despite the fact that the magnitudes of the molecular coefficients in case 3 are much larger than those in case 4. To explain these observations, it is useful to compare the evolution of $\langle VD/\mu \rangle$ for cases 3 and 4. In case 4, $\langle VD/\mu \rangle = \langle VD \rangle$. Figure 13(b) shows that the magnitudes of $\langle VD/\mu \rangle$ in case 3 are significantly lower than those in case 4. In case 3, the values of μ are higher, the “smoothing” effects of the molecular viscosity on the velocity gradients are more important, and the magnitudes of $\langle VD/\mu \rangle$ decay faster. This explains why the long time values of $\langle VD \rangle$ in case 3 are smaller than those in case 4.

The influence of the heat of reaction and the flow compressibility on the viscous-dissipation and the pressure-dilatation terms is further assessed in Fig. 14, where the time integrated values of $\langle PD \rangle$ and $\langle VD \rangle$ for several different cases are considered. The variation in the mean kinetic energy is equal to the summation of these integrated quantities. Figure 14(a) shows that in non-heat-releasing cases the integrated values of the pressure-dilatation term are relatively small. In the heat-releasing cases, these integrated values are positive and significant. While flow compressibility has little effect in non-heat-releasing cases, it significantly amplifies the effect of reaction on the integrated values of the pressure dilatation in heat-releasing cases (compare cases 1, 2, 6, and 9). The positive sign of the integrated values of the pressure-dilatation term indicates that this term on the average re-

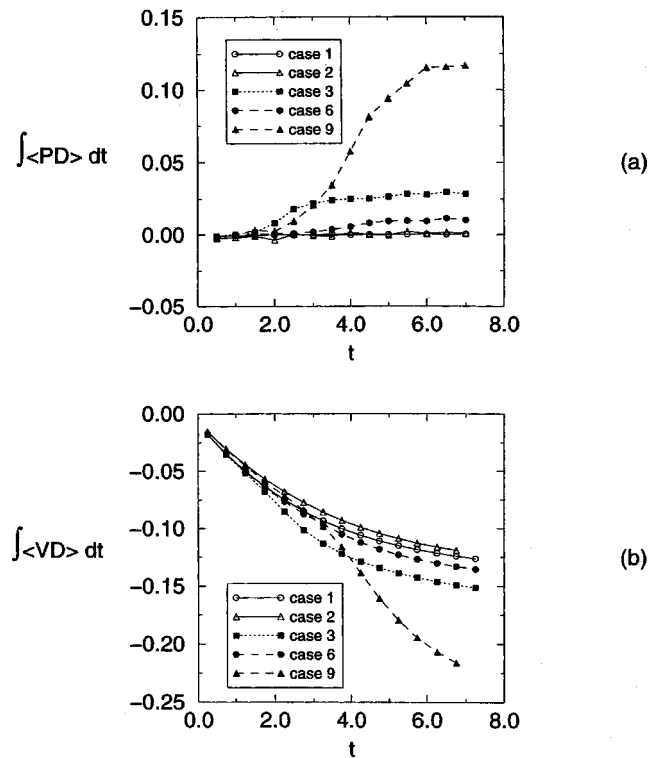


FIG. 14. Time-integrated values of different terms in the mean kinetic energy equation [Eq. (14)], (a) the pressure dilatation, (b) the viscous dissipation.

moves energy from the internal energy and adds it to the kinetic energy. In the exothermic reacting flows, as the results in Fig. 14(a) suggest, the role of the pressure-dilatation term is very important and should be considered in the modeling of these flows, particularly when the flow compressibility is significant.

In contrast to the pressure dilatation, the integrated values of the viscous-dissipation term are always negative and increase in magnitude as heat release increases [Fig. 14(b)]. In non-heat-releasing cases, the magnitudes of this quantity decrease as the initial flow compressibility increases, which is consistent with the results shown in Fig. 12. However, in heat-releasing cases the flow compressibility has an opposite effect and enhances the magnitude of the viscous dissipation. This is primarily due to an increase in the dilatational turbulent motions (see the discussion corresponding to Fig. 15 below).

It is shown above that the turbulent kinetic energy and the terms responsible for its evolution are noticeably affected by the heat of reaction. However, the results in Figs. 10 and 11 indicate that the solenoidal and the dilatational components of the turbulent energy are affected differently by the reaction. It is, therefore, useful to consider the evolution equations for the solenoidal and dilatational energy components. Analysis of these transport equations also helps to better understand the energy transfer process in reacting flows. The interactions between different modes of the kinetic energy and the internal energy in compressible flows are studied in detail by Kida and Orszag,⁴⁴ and Jaberi and Madnia.³⁷ They decompose $W_i = \sqrt{\rho} u_i$ into the mean, the

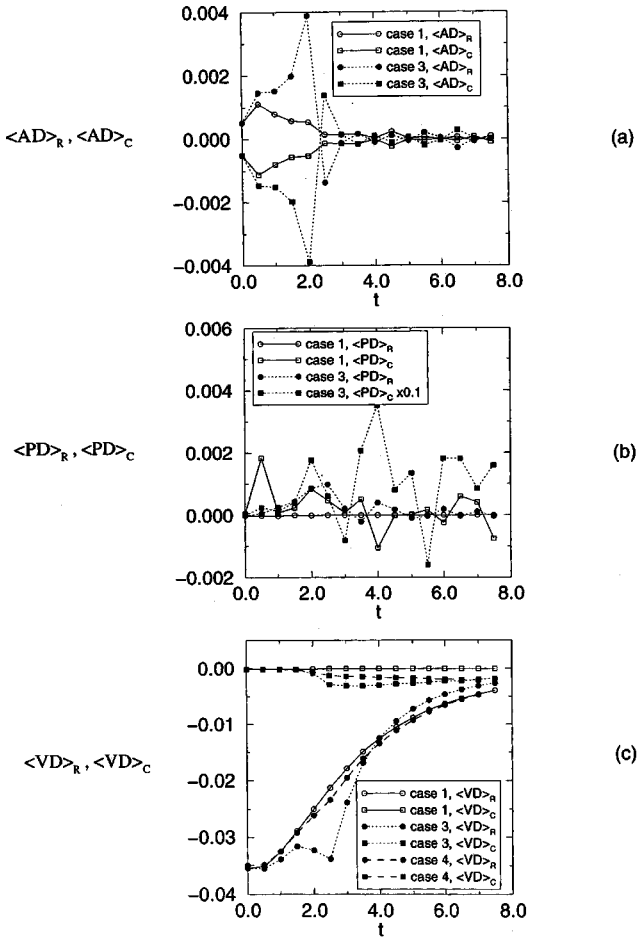


FIG. 15. Temporal variation of the rotational and the compressive components of (a) the advection term, (b) the pressure-dilatation term, and (c) the viscous-dissipation term.

rotational, and the compressive components. Similar analysis is conducted here. The decomposition of the kinetic energy and also the governing equations describing the evolution of the compressive and rotational components of the kinetic energy for constant molecular transport coefficients are provided by Kida and Orszag⁴⁴ and are not given in detail here. It is only adequate to present the evolution equations of the spatially averaged values of the kinetic energy components. These equations are written as

$$\frac{d}{dt} \langle (E_K)_\beta \rangle = \langle (AD)_\beta \rangle + \langle (PD)_\beta \rangle + \langle (VD)_\beta \rangle, \quad (15)$$

where $(E_K)_\beta$, $\beta \equiv R, C, O$ denotes the rotational, the compressive, and the mean components of the kinetic energy, respectively. In Eq. (15), $\langle (AD)_\beta \rangle$, $\langle (PD)_\beta \rangle$, and $\langle (VD)_\beta \rangle$ represent the effect of the advection, the pressure dilatation, and the viscous dissipation on the volumetric averaged values of the kinetic energy components and are defined as⁴⁴

$$\langle (AD)_\beta \rangle \equiv \left\langle \left(-u_j \frac{\partial W_i}{\partial x_j} - \frac{1}{2} W_i \Delta \right) W_{\beta i} \right\rangle, \quad (16)$$

$$\langle (PD)_\beta \rangle \equiv \left\langle -\frac{1}{\sqrt{\rho}} \frac{\partial p}{\partial x_i} W_{\beta i} \right\rangle,$$

$$\langle (VD)_\beta \rangle \equiv \left\langle \left(\frac{2}{\text{Re}_o \sqrt{\rho}} \frac{\partial}{\partial x_j} \left[\mu \left(S_{ij} - \frac{1}{3} \Delta \delta_{ij} \right) \right] \right) W_{\beta i} \right\rangle,$$

where $W_{\beta i}$, $\beta \equiv R, C, O$ denotes the rotational, the compressive, and the mean components of W_i , respectively. Our results (not shown) indicate that in both non-heat-releasing and heat-releasing cases the mean components of the advection, $\langle (AD)_O \rangle$, the pressure dilatation $\langle (PD)_O \rangle$, and the viscous dissipation, $\langle (VD)_O \rangle$, are negligible as compared to the compressive and rotational counterparts.

Temporal variations of the rotational and the compressive components of the advection term for both non-heat-releasing and heat-releasing cases are considered in Fig. 15(a). This figure shows that in the absence of heat release, the compressive and the rotational components of the advection term fluctuate symmetrically with respect to the horizontal (zero-value) axis and there is no net contribution to the kinetic energy by these components. In the case with considerable heat release, again the compressive and the rotational components fluctuate symmetrically around the horizontal axis but the amplitude of their oscillations is larger than that in the non-heat-releasing case. Additionally, during the time period that the reaction is significant, the time averaged values of $\langle (AD)_R \rangle$ and $\langle (AD)_C \rangle$ are positive and negative, respectively. These results are consistent with those of Jaber and Madnia³⁷ and indicate that on the average, the energy is transferred from the compressive component of the kinetic energy to its rotational component. To explain this behavior, it is useful to consider the mechanisms responsible for the change in the dilatational fluid motions. In compressible non-reacting flows, the compressibility effects caused by initial conditions or other factors, such as shock waves, enhance the dilatational turbulent motions.⁴⁴ The solenoidal fluid motions may also amplify the dilatational fluid motions through the advection term. Alternatively, the energy could be transferred from the dilatational motions to solenoidal motions by the dilatational advection which is the case in our nonreacting simulations. In reacting flows, the heat of reaction modifies the dilatational fluid motions. The modified dilatational field then may affect the solenoidal field. The direction of the energy transfer between the solenoidal and the dilatational components of the kinetic energy depends on the rate of heat release and the energy residing in each component. In case 3, the energy released by the reaction is noticeably large and the net energy transfer is from the dilatational component to the solenoidal component.

The temporal variations of the rotational and the compressive components of the pressure dilatation for cases 1 and 3 are considered in Fig. 15(b). It is the pressure-dilatation term that alternatively transfers energy from the internal energy to dilatational and solenoidal parts of the kinetic energy and vice versa. The results in Fig. 15(b) show that in the non-heat-releasing case, the rotational component of the pressure dilatation is negligible, indicating that the pressure dilatation does not transfer energy to or from the rotational kinetic energy. In the case with considerable heat release, the values of $\langle (PD)_C \rangle$ and $\langle (PD)_R \rangle$ oscillate around zero but the amplitude of oscillations is significantly higher

than in the nonreacting case. Again, consistent with the results of Jaberi and Madnia,³⁷ the compressive component of the pressure dilatation has magnitudes substantially larger than those of the rotational component. The cases with higher initial flow compressibility exhibit behavior similar to that shown in Fig. 15(b). The variation of the pressure-dilatation term in Figs. 13(a) and 14(a) with reaction and flow compressibility is mainly due to variation of its dilatational component as the solenoidal component is not noticeably affected. The dilatational component of the pressure dilatation changes in magnitude with reaction and flow compressibility.

The influence of reaction on different components of the viscous-dissipation term is shown in Fig. 15(c). In the absence of heat release, the magnitude of the rotational and compressive components of the viscous dissipation decrease with turbulence decay. In this case, the magnitudes of $\langle (VD)_R \rangle$ are much larger than those of $\langle (VD)_C \rangle$, suggesting that the dissipation scales are controlled by the vortical motions. Nevertheless, Fig. 15(c) shows that both the rotational and the compressive components are significantly affected by the reaction, although the compressive component is affected more. It is observed that the magnitudes of the $\langle (VD)_R \rangle$ in heat-releasing case 3 are higher than those in non-heat-releasing case 1 at $t < 4$. The increase in solenoidal dissipation is primarily due to the increase in molecular coefficients with temperature, since the results for cases 1 and 4 are close. The increase in dilatational dissipation is due to both enhancement of the small-scale dilatational velocity fluctuations and increase in molecular coefficients. A comparison between the results in cases 1, 3, and 4 indicates that the magnitudes of $\langle (VD)_C \rangle$ increase by almost an order of magnitude with reaction, even if the molecular coefficients are kept constant. Additionally, the magnitudes of $\langle (VD)_C \rangle$ decay slowly as compared to those of $\langle (VD)_R \rangle$. Consequently, the long time values of the rotational and the compressive dissipation become comparable. Our results (not shown) also indicate that the temporal evolution of $\langle (VD)_R \rangle$ is not very much dependent on the initial flow compressibility in non-heat-releasing cases. However, the values of $\langle (VD)_C \rangle$ are higher and are enhanced more by the heat of reaction in cases with higher initial flow compressibility.

D. Enstrophy

The results shown in Fig. 11 indicate that different scales of the solenoidal and the dilatational velocity fluctuations are affected differently by the chemical reaction. While all length scales of the dilatational velocity field are amplified, the small-scale solenoidal motions are primarily affected by the reaction. An important quantity which characterizes these small-scale solenoidal motions is the enstrophy. The temporal variation of the mean enstrophy for several different cases is shown in Fig. 16. In the absence of heat release, $\langle \Omega \rangle$ decays monotonically (and almost exponentially) due to viscous dissipation. However, the heat of reaction influences the mean enstrophy and $\langle \Omega \rangle$ decays much faster in heat-releasing case 3. To isolate the effect of reaction on the molecular viscosity coefficient from other factors that affect $\langle \Omega \rangle$, in Fig.

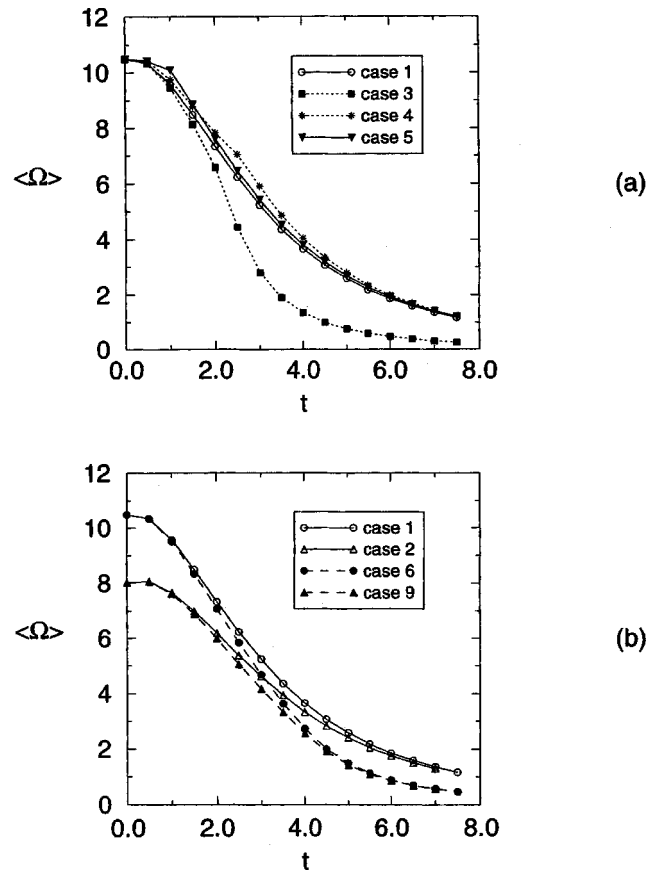


FIG. 16. Temporal variation of the mean enstrophy for different cases.

16(a) the temporal evolution of $\langle \Omega \rangle$ for cases 4 and 5 is also considered. The results corresponding to these cases clearly indicate that the values of $\langle \Omega \rangle$ are affected by the heat release, primarily due to variations in the molecular transport coefficients. A comparison between cases 1 and 3 in Figs. 16(a) and 10(b) indicates that the effect of reaction on the enstrophy is more significant than that on the solenoidal kinetic energy. This is understandable since the small (dissipative) flow scales are affected the most.

In contrast to dilatational turbulent motions, the small-scale solenoidal motions are affected similarly by the reaction for different initial flow compressibility. This is demonstrated in Fig. 16(b), where the decay of the mean enstrophy for cases 1, 2, 6, and 9 are considered. Figure 16(b) is consistent with Fig. 16(a) and shows that the reaction increases the decay rate of the mean enstrophy, regardless of the initial flow compressibility. As mentioned before, initially the summation of the dilatational and solenoidal turbulent energies is the same in all cases. But in cases 2 and 9, the initial values of the solenoidal energy and enstrophy are lower than those in cases 1 and 6. Nevertheless, the long time values of the mean enstrophy in cases 1 and 2 and also those in cases 6 and 9 are very close. The solenoidal kinetic energy, although affected less by the reaction, exhibits a qualitatively similar behavior. These results suggest that in reacting and nonreacting flows the long time values of the ‘‘solenoidal statistics’’ are independent of the initial flow compressibility. Of course

they are affected by the reaction, primarily due to variations in molecular coefficients.

1. Enstrophy transport equation

To understand how the chemical reaction affects the vorticity field and to explain the results in Fig. 16, the terms in the enstrophy transport equation are examined. The transport equation for mean enstrophy reads as

$$\begin{aligned} \frac{d\langle\Omega\rangle}{dt} = & \underbrace{-\langle\boldsymbol{\omega}\cdot\underline{S}\cdot\boldsymbol{\omega}\rangle}_{\text{term I}} - \underbrace{\langle\Omega\Delta\rangle}_{\text{term II}} - \underbrace{\left\langle\frac{1}{\rho^2}[\boldsymbol{\omega}\cdot(\nabla p\times\nabla\rho)]\right\rangle}_{\text{term III}} \\ & + \underbrace{\frac{2}{\text{Re}_o}\langle\boldsymbol{\omega}\cdot[\nabla\times(\underline{\xi}^s/\rho)]\rangle}_{\text{term IV}} + \underbrace{\frac{2}{\text{Re}_o}\langle\boldsymbol{\omega}\cdot[\nabla\times(\underline{\xi}^d/\rho)]\rangle}_{\text{term V}}, \end{aligned} \quad (17)$$

where $\boldsymbol{\omega}$ and \underline{S} are the vorticity vector and strain rate tensor, respectively. The solenoidal and the dilatational viscous forces are defined as

$$\begin{aligned} \underline{\xi}^s & \equiv \nabla\cdot(\mu\underline{S}^s), \\ \underline{\xi}^d & \equiv \nabla\cdot\left(\mu\underline{S}^d - \frac{\mu}{3}\Delta\underline{I}\right), \end{aligned} \quad (18)$$

where \underline{S}^s and \underline{S}^d denote the solenoidal and the dilatational strain rates, and \underline{I} is the identity tensor, respectively. Terms I, II, III, IV, and V on the right-hand side (rhs) of Eq. (17) are identified as the vortex-stretching, the vorticity-expansion, the baroclinic, the solenoidal-dissipation, and the dilatational-dissipation terms, respectively. The vortex-stretching term is responsible for energy transfer among different turbulent scales and usually has a positive sign. The vorticity-expansion term can have a positive or negative contribution to the mean enstrophy, depending on the correlation between the contraction/expansion regions of the flow and the local values of the enstrophy. The baroclinic term changes the mean enstrophy only if the pressure gradient and the density gradient vectors are not aligned. The solenoidal and the dilatational viscous terms decrease the magnitude of mean enstrophy. In low Mach number nonreacting flows, the dilatational-dissipation term is usually negligible.

Temporal evolution of all terms on the rhs of Eq. (17) for cases 1 and 3 are shown in Fig. 17. In the non-heat-releasing case 1 [Fig. 17(a)], the magnitudes of the vorticity-expansion, the baroclinic, and the dilatational-dissipation terms are relatively small and the mean enstrophy mainly changes by the vortex-stretching and the solenoidal-dissipation terms, as expected for a nearly incompressible flow. The vortex-stretching term has a positive sign and its magnitudes are slightly lower than those of the solenoidal dissipation. As a result, the mean enstrophy decays continuously. The vorticity-expansion and the baroclinic terms oscillate around zero. In the heat-releasing case 3 [Fig. 17(b)], the vortex-stretching and the solenoidal-dissipation terms are still the dominant terms and decrease in magnitude with turbulence decay. However, a comparison between the results

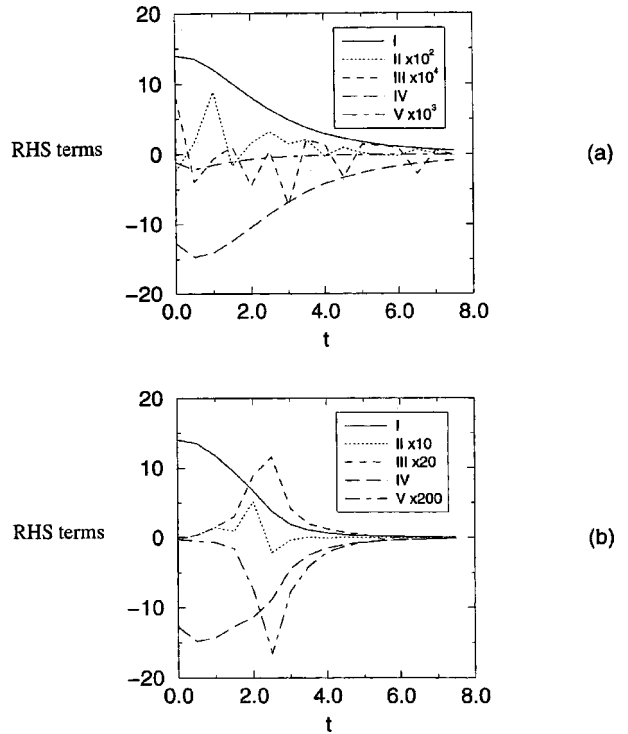


FIG. 17. Temporal variation of different terms in the mean enstrophy transport equation [Eq. (17)] for (a) case 1, (b) case 3.

in Figs. 17(a) and 17(b) indicates that these terms decay faster in heat-releasing case 3. This is due to higher values of the molecular coefficients in the heat-releasing case. Also, in the heat-releasing case, the magnitudes of terms II, III, and V are comparatively higher than those in the non-heat-releasing case. The baroclinic term is positive and peaks when the mean reaction rate reaches its maximum value. The vorticity-expansion term has magnitudes comparable to the baroclinic term but contributes both positively and negatively to the mean enstrophy. The magnitude of the dilatational-dissipation term also peaks when the mean reaction rate peaks but is lower than that of the vorticity-expansion and baroclinic terms.

The integrated values of all terms on the rhs of Eq. (17) are shown in Fig. 18 for various cases. The summation of these integrated quantities is equal to the change in the magnitude of the mean enstrophy. The results in Fig. 18 are consistent with those in Fig. 17, indicating that all terms on the rhs of Eq. (17) are affected by the heat release. A comparison between the results for cases 1 and 3 in Fig. 18(a) indicates that the integrated value of the vortex-stretching term is significantly decreased by the reaction and reaches a nearly constant value at $t > 4$. This is primarily due to variation of the molecular coefficients with temperature, as the results for cases 1 and 4 are very close. In contrast to the vortex-stretching term, the integrated values of the vorticity-expansion and baroclinic terms increase substantially by the heat of reaction. The values of the vorticity-expansion term are lower when the molecular coefficients are kept constant (compare cases 3 and 4). The baroclinic term exhibits opposite behavior as its integrated values are increased more significantly by the reaction if the molecular coefficients are

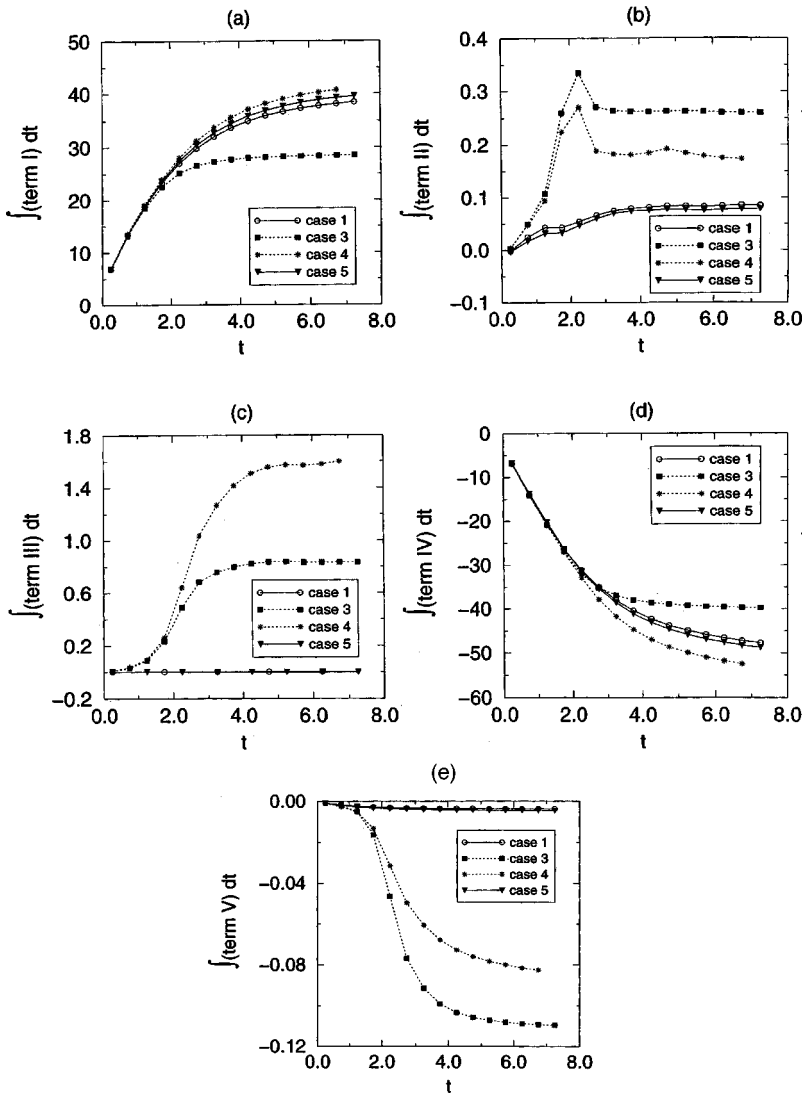


FIG. 18. Time-integrated values of different terms in Eq. (17) contributing to the mean enstrophy, (a) term I, (b) term II, (c) term III, (d) term IV, (e) term V.

kept constant. This indicates that the increase in magnitudes of the molecular coefficients weakens the baroclinic generation of the mean enstrophy.

The solenoidal- and the dilatational-dissipation terms are also affected differently by the heat of reaction. While the magnitudes of the solenoidal dissipation decrease by the reaction [Fig. 18(d)], those of the dilatational dissipation increase [Fig. 18(e)]. Figures 18(d) and 18(e) also show that the magnitudes of the (solenoidal-) dilatational-dissipation term in case 4 are (higher) lower than those in case 3. So, the variation of the molecular coefficients with temperature has the opposite effect on these two viscous terms. The results in Fig. 18(d) are also consistent with those in Fig. 18(a) and indicate that the magnitudes of the solenoidal-dissipation and the vortex-stretching terms decrease by reaction due to enhancement of the molecular coefficients. In contrast, the magnitudes of the vorticity-expansion and the dilatational-dissipation terms increase as the magnitudes of the molecular coefficients increase. It is to be noted that even though the vorticity-expansion, the baroclinic, and the dilatational-dissipation terms are strongly affected by reaction, their contributions to the mean enstrophy remain much less than those of the vortex-stretching and the solenoidal-dissipation terms

in all cases. Our results (not shown) suggest that in exothermic reacting flows while the magnitudes of the baroclinic and the dilatational-dissipation terms are dependent on the initial flow compressibility, the vortex-stretching and the solenoidal-dissipation terms are not noticeably affected by the compressibility. Therefore, the effects of the reaction on the mean enstrophy as shown in Fig. 16(b) are similar in cases with different initial flow compressibility.

Generation of vorticity via baroclinic torque plays an important role in the flame-vortex interactions.^{48,60,61} Although in the flows studied the baroclinic term does not significantly change the mean enstrophy, it has important local effects on the vorticity field and the flame structure. In the mean enstrophy transport equation, the baroclinic term, $-\langle 1/\rho^2[\boldsymbol{\omega} \cdot (\nabla p \times \nabla \rho)] \rangle$ is composed of three vectors; both the magnitude and relative alignment of these are important. The magnitudes of the pressure and the density gradients increase as the pressure and the density fluctuations are increased by reaction. This is shown in Fig. 19(a), where the volumetric averaged values of the magnitudes of the density and the pressure gradients for cases 1, 3, and 6 are considered. The mean value of $1/\rho^2$ follows closely the trends observed in Fig. 19(a) for density gradient but its magnitudes

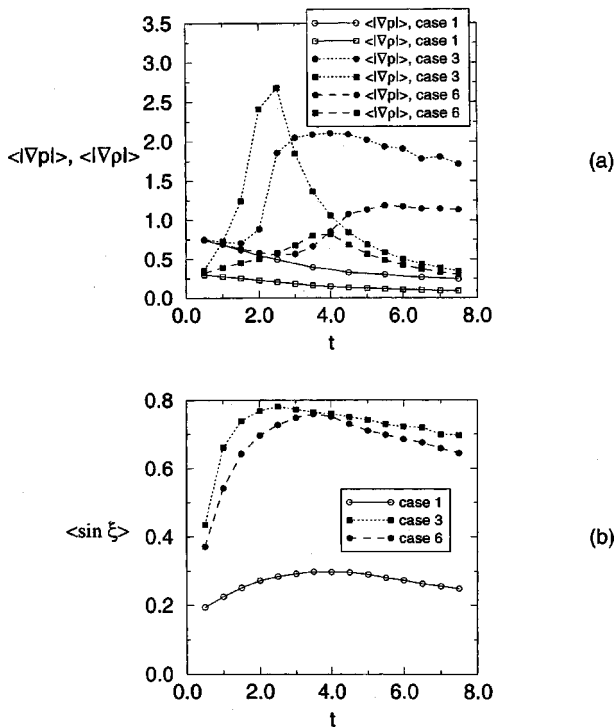


FIG. 19. Time variation of (a) the magnitudes of the density and the pressure gradients, (b) average of the sine of the angle between the pressure gradient and the density gradient.

are increased by less than 15% with reaction. For the isothermal reacting cases, both $\langle |\nabla \rho| \rangle$ and $\langle 1/\rho^2 \rangle$ decrease slowly and continuously due to turbulence decay. In exothermic reacting cases, they peak at the time corresponding to peak reaction rate and decay later. The decrease in the magnitude of the vorticity vector is somewhat balanced by the increase in $\langle 1/\rho^2 \rangle$ in heat-releasing cases. This decrease in $|\omega|$, as explained earlier, is due to an increase in molecular coefficients with temperature.

The second factor which influences the magnitude of the baroclinic term is the alignment of the pressure and the density gradient vectors. The time evolution of the mean value of $\sin \xi$ (ξ is the angle between the pressure and the density gradient vectors) is presented in Fig. 19(b). The results in this figure clearly indicate that the reaction has a significant influence on the alignment of these two vectors as $\langle \sin \xi \rangle$ increases with reaction. At the time which the mean reaction rate peaks, the density and the pressure gradient vectors tend to be mostly perpendicular. To further examine this behavior, in Fig. 20(a) the PDFs of $\sin \xi$ for cases 1 and 3 are compared. The results for case 1 are consistent with those obtained by Kida and Orszag⁶² and indicate that the pressure and the density gradients are almost aligned. This alignment is also supported by the high correlation between the pressure and the density which is a consequence of a nearly isentropic process. The PDF of $\sin \xi$ is changed by the heat release and attains a peak at $\sin \xi \approx 1$ and very low values at $\sin \xi \approx 0$. This indicates that in most of the domain the pressure and the density gradients are perpendicular. Our results (not shown) also indicate that the pressure and the density

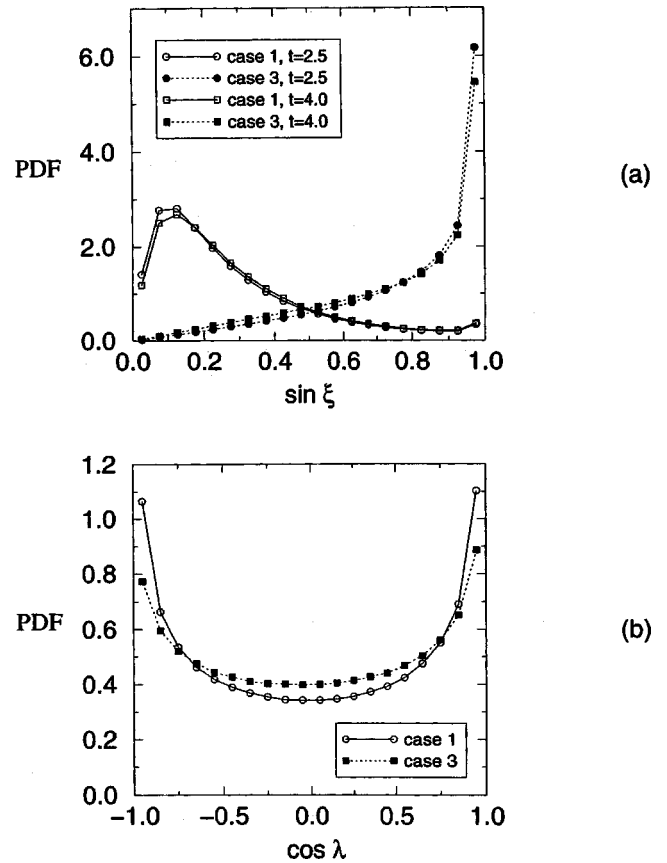


FIG. 20. PDFs of (a) the sine of angle between the pressure gradient and the density gradient, (b) the cosine of angle between the vorticity vector and ψ .

fluctuations are poorly correlated when the heat release is significant.

Another quantity which influences the behavior of the baroclinic term is the angle between the vorticity vector and the baroclinic torque ($\psi = -\nabla p \times \nabla \rho$). The PDFs of the cosine of this angle ($\cos \lambda$) at $t=2.5$ are shown in Fig. 20(b). The highest probability is at ± 1 , indicating that ψ and ω are mostly parallel. In case 1, the PDF is nearly symmetric and the mean value of $\cos \lambda$ is very small. In case 3, the PDF is slightly skewed toward positive values at $1.5 < t < 3.5$. Consequently, the mean value of $\cos \lambda$ is positive and small.

E. Dilatation

It is demonstrated above that the dilatational turbulent motions are substantially modified by the heat of reaction. An important quantity which characterizes the small-scale dilatational turbulent motion is the second moment of dilatation ($\langle \Delta^2 \rangle$). This term is almost equal to the dilatation variance since the mean value of the dilatation is nearly zero. Figure 21 shows the temporal variation of $\langle \Delta^2 \rangle$ for various cases. In the non-heat-releasing case, the values of $\langle \Delta^2 \rangle$ are higher for higher initial flow compressibility but decrease in all cases with turbulence decay. The results in Fig. 21 are also consistent with those shown in Figs. 10(c) and 11(b) and indicate that the magnitudes of $\langle \Delta^2 \rangle$ increase substantially

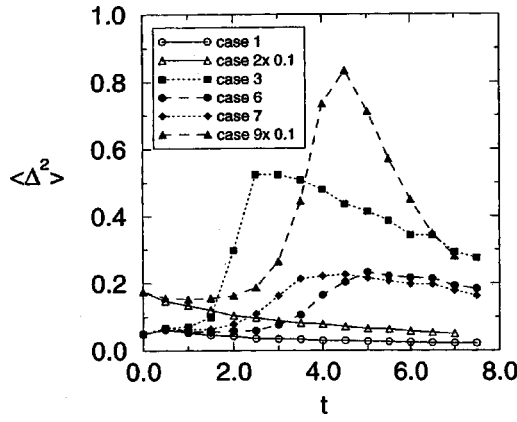


FIG. 21. Temporal variation of the second moment or variance of the dilatation for different cases.

with the heat of reaction. This increase is dependent on the rate of heat release and is more significant in cases with higher initial flow compressibility.

To understand how the dilatational fluid motions are affected by the reaction, the transport equation for $\langle \Delta^2 \rangle$ is considered,

$$\begin{aligned} \frac{d\langle \Delta^2 \rangle}{dt} = & \underbrace{\langle \Delta^3 \rangle}_{\text{term I}} - 2 \underbrace{\langle \Delta S_{ij} S_{ij} \rangle}_{\text{term II}} + \underbrace{\langle \Delta \omega_k \omega_k \rangle}_{\text{term III}} \\ & + 2 \underbrace{\left\langle \frac{1}{\rho} \frac{\partial p}{\partial x_j} \frac{\partial \Delta}{\partial x_j} \right\rangle}_{\text{term IV}} \\ & - \underbrace{\frac{4}{\text{Re}_o} \left\langle \frac{1}{\rho} \frac{\partial (\mu S_{ij})}{\partial x_i} \frac{\partial \Delta}{\partial x_j} \right\rangle}_{\text{term V}} + \underbrace{\frac{4}{3 \text{Re}_o} \left\langle \frac{1}{\rho} \frac{\partial (\mu \Delta)}{\partial x_j} \frac{\partial \Delta}{\partial x_j} \right\rangle}_{\text{term VI}}. \end{aligned} \quad (19)$$

Temporal evolution of the terms on the rhs of Eq. (19) for cases 1, 2, and 9 are shown in Fig. 22. In case 1 [Fig. 22(a)], the flow is nearly incompressible and the magnitude of $\langle \Delta^2 \rangle$ and all terms contributing to its evolution are very small and decline with the decay of turbulence. Term II represents the correlation between the dilatation and the magnitude of the strain and tends to decrease $\langle \Delta^2 \rangle$. Term III represents the correlation between the enstrophy and the dilatation and also appears in the enstrophy transport equation multiplied by $-1/2$. This term has both negative and positive contribution but its time integrated values are mostly negative. Term IV represents the correlation between the pressure gradient and the dilatation gradient. This term has the most significant influence on $\langle \Delta^2 \rangle$ and always enhances the fluctuations of the dilatation. The two viscous terms have opposite effects on $\langle \Delta^2 \rangle$. The first term (term V) represents the correlation between the gradient of the dilatation and the strain rate. The second term (term VI) is due to dilatation gradient and has magnitudes slightly lower than the first term. While the values of $\langle \Delta^2 \rangle$ decrease by the first viscous term, the second term increases them.

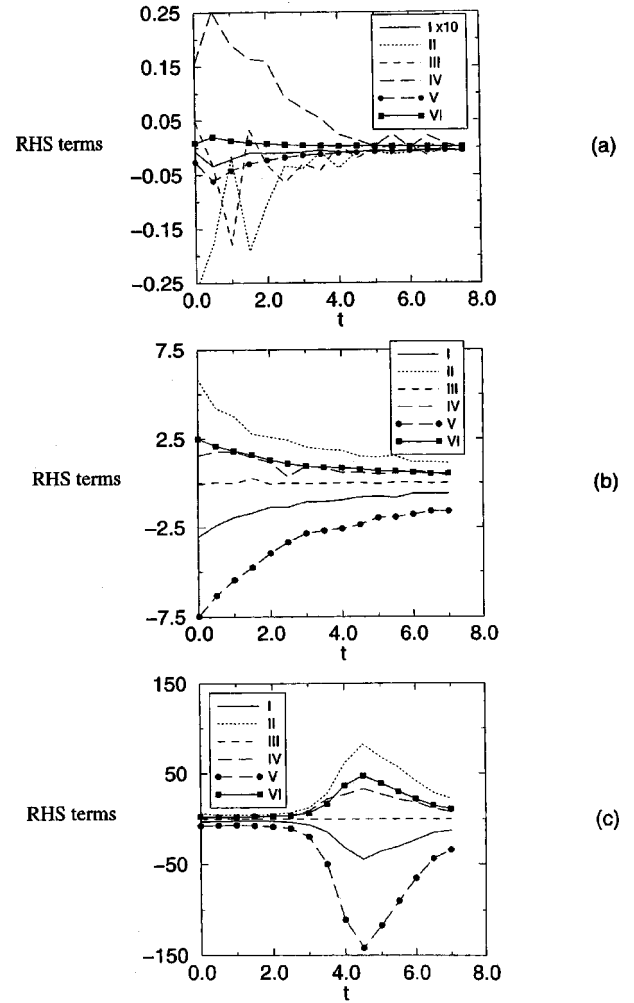


FIG. 22. Temporal variation of different terms in Eq. (19) contributing to the second moment of dilatation (a) case 1, (b) case 2, (c) case 9.

A comparison between cases 1 and 2 in Figs. 22(a) and 22(b) reveals the effects of compressibility on terms on the rhs of Eq. (19). While in case 1 the values of term III are comparable to other terms, they are relatively insignificant in case 2. This suggests that the correlation between the dilatation and the solenoidal velocity fields is small and is not significantly affected by the flow compressibility. The flow compressibility has, however, a significant effect on other terms. For example, the magnitudes of term I in case 2 are much higher than those in case 1. In both cases this term has a negative contribution. The behavior of term II is also very different in cases 1 and 2. This term decreases the fluctuations of the dilatation in case 1. In the cases with significant initial compressibility (case 2), the reverse is true and term II has the most significant positive contribution. The magnitude of term IV increases substantially by the flow compressibility, as expected. The viscous terms V and VI exhibit similar behavior in cases 1 and 2. Term V always contributes negatively to the values of $\langle \Delta^2 \rangle$ but the contribution of term VI is always positive. The magnitudes of term V are larger than those of VI resulting in a net negative contribution to the dilatation variance by the viscous terms.

It is shown in Fig. 21 that the values of $\langle \Delta^2 \rangle$ are signifi-

cantly affected by the heat of reaction. It is, therefore, not surprising that all terms contributing to $\langle \Delta^2 \rangle$ are also affected by the reaction. In fact, Fig. 22(c) shows that with the exception of term III the magnitudes of all terms on the rhs of Eq. (19) increase by more than an order of magnitude with reaction. Nevertheless, the behavior is similar in non-heat-releasing and heat-releasing cases 2 and 9, indicating that terms II and V have the most significant positive and negative contributions, respectively. Close examination of the results in Figs. 22(b) and 22(c) indicates that the values of term III in cases 2 and 9 are small and comparable. This again suggests that the vortical and the dilatational velocity fields are weakly correlated.

IV. SUMMARY AND CONCLUSIONS

Direct numerical simulations are conducted of chemically reacting homogeneous compressible fluid flow under non-heat-releasing (isothermal) and heat-releasing (exothermic) non-premixed reacting conditions. The chemistry is modeled with a one-step irreversible reaction and with a rate coefficient of an Arrhenius type.

Examination of the compositional flame structure indicates that the finite rate chemistry (or temperature dependency) effects are important and the reaction rate exhibits behavior different than the flame surface density. During the time that the reaction is significant, the "mixing" term ($G = \rho^2 Y_A Y_B$) and the "temperature-dependent" term [$F = \exp(-Ze/T)$] have comparable mean values. Also, at this time the mixing term is not well correlated with the reaction rate. While the values of the temperature-dependent term are high at the "reaction zones," those of the mixing term are dependent on the spatial density variations and are often low in these zones. Additionally, in the reaction zones the flow is dominated by strain rather than rotation and the scalar gradient is mostly aligned with the most compressive eigenvector of the strain rate tensor. Consistent with the previous observations, the heat of reaction decreases the alignment between intermediate strain eigenvector and vorticity vector, particularly near the reaction zones.

The results of simulations with isothermal reaction are in accord with the previous findings and indicate that the flow undergoes a nearly isentropic process and the pressure and density fluctuations are very well correlated. However, in exothermic reacting simulations, the dilatational (compressive) turbulent motions at all length scales are significantly intensified by the heat of reaction. The effect of reaction on the dilatational velocity field is enhanced as the initial flow compressibility (the initial fluctuations in dilatational velocity and thermodynamic variables) increases. Analysis of the transport equation for dilatation variance ($\langle \Delta^2 \rangle$) indicates that the magnitudes of $\langle \Delta^2 \rangle$ and almost all terms contributing to its evolution increase substantially with increase in the initial flow compressibility and/or the heat of reaction. The exothermicity of the reaction also increases the fluctuations of the thermodynamic variables at all length scales.

In contrast to the dilatational velocity field, the low order moments of the solenoidal (rotational) velocity field and the scalars are not significantly affected by the reaction. This is

because the large-scale solenoidal velocity field is not directly affected by the reaction and the solenoidal and dilatational velocity fields are poorly correlated. However, the small-scale rotational turbulent motions and the related quantities such as the enstrophy are noticeably influenced by the heat of reaction. This is primarily due to variation of the molecular transport coefficients with temperature and the volumetric flow expansion/contraction has lesser effect. Analysis of the enstrophy transport equation indicates that the effects of baroclinic torque increase as the heat release and/or the initial flow compressibility increases. Nevertheless, the contributions of the baroclinic torque and the vorticity expansion are much less than those of the vortex-stretching and the solenoidal viscous-dissipation.

Examination of the energy transfer among different modes of the kinetic energy and the internal energy in exothermic reactive flows indicates that the energy of the reaction is transferred to the compressive component of the kinetic energy by the compressive component of the pressure-dilatation correlations. The advection term then transfers the energy from the compressive component of the kinetic energy to its rotational component. The compressive and the rotational components of the turbulent advection and the compressive component of the pressure-dilatation exhibit significant oscillations in time. The amplitude of these oscillations enhances due to the heat of reaction. The compressive component of the viscous dissipation also increases in magnitude as a result of the energy transfer from the internal energy to the compressive component of the kinetic energy. The effects of reaction on pressure dilatation and viscous dissipation increase with the flow compressibility due to strong coupling between the "turbulence-generated" and the "heat-generated" dilatational fluid motions. Also, in all cases considered, the rotational and the compressive components of the kinetic energy are poorly correlated.

The results presented in this paper reveal the intricate physics of the two-way interactions between turbulence and chemical reaction. The future models of the turbulent reacting flows have to account for these interactions. We are utilizing the DNS results obtained from this work to develop new subgrid scale models in Large Eddy Simulations (LES) of turbulent reacting flows. We are specifically interested in how the subgrid stresses and scalar fluxes and the corresponding models in LES are affected by the chemical reaction. The behavior of the subgrid unmixedness in reacting flows is also of interest and is being studied using the data of this work.

In this study, the turbulent Mach number and the flow compressibility are relatively small. The turbulence is also decaying due to lack of any mean velocity gradient or shear. Analysis of the flame-turbulence interactions in highly compressible and supersonic homogeneous and inhomogeneous chemically reactive turbulent flows would be the next challenging tasks.

ACKNOWLEDGMENTS

This work was sponsored by the National Science Foundation under Grant No. CTS-9623178. Computational re-

sources were provided by the San Diego Supercomputer Center, National Center for Supercomputer Applications at the University of Illinois Urbana-Champaign, and the Center for Computational Research at the State University of New York at Buffalo.

- ¹P. Givi, "Model free simulations of turbulent reactive flows," *Prog. Energy Combust. Sci.* **15**, 1 (1989).
- ²S. B. Pope, "Computations of turbulent combustion: Progress and challenges," in *Proceedings of 23rd Symposium (Int.) on Combustion* (The Combustion Institute, Pittsburgh, PA, 1990), pp. 591-612.
- ³*Turbulent Reacting Flows*, edited by P. A. Libby and F. A. Williams (Academic, London, 1994).
- ⁴R. O. Fox, "Computational methods for turbulent reacting flows in chemical process industry," *Rev. Inst. Français Petrole* **51**(2), 215 (1996).
- ⁵L. Vervisch and T. Poinsot, "Direct numerical simulation of non-premixed turbulent flames," *Annu. Rev. Fluid Mech.* **330**, 655 (1998).
- ⁶W. C. Strahle, "Duality, dilation, diffusion and dissipation in reacting turbulent flows," in *Proceedings of 19th Symposium (Int.) on Combustion* (The Combustion Institute, Pittsburgh, PA, 1982), pp. 337-347.
- ⁷P. A. McMurtry, W.-H. Jou, J. J. Riley, and R. W. Metcalfe, "Direct numerical simulations of a reacting mixing layer with chemical heat release," *AIAA J.* **24**, 962 (1986).
- ⁸S. M. Masutani and C. T. Bowman, "The structure of a chemically reacting plane mixing layer," *J. Fluid Mech.* **72**, 93 (1986).
- ⁹P. A. McMurtry, J. J. Riley, and R. W. Metcalfe, "Effects of heat release on the large scale structures in a turbulent reacting mixing layer," *J. Fluid Mech.* **199**, 297 (1989).
- ¹⁰J. C. Hermanson and P. E. Dimotakis, "Effects of heat release in a turbulent, reacting shear layer," *J. Fluid Mech.* **199**, 333 (1989).
- ¹¹P. Givi, C. K. Madnia, C. J. Steinberger, M. H. Carpenter, and J. P. Drummond, "Effects of compressibility and heat release in a high speed reacting mixing layer," *Combust. Sci. Technol.* **78**, 33 (1991).
- ¹²F. F. Grinstein and K. Kailasanath, "Chemical energy release and dynamics of transitional, reactive shear flows," *Phys. Fluids A* **4**, 2207 (1992).
- ¹³R. S. Miller, C. K. Madnia, and P. Givi, "Structure of a turbulent reacting mixing layer," *Combust. Sci. Technol.* **99**, 1 (1994).
- ¹⁴P. E. Dimotakis, "Turbulent free shear layer mixing and combustion," in *High Speed Flight Propulsion Systems, Progress in Astronautics and Aeronautics*, edited by S. N. B. Murthy and E. T. Curran (AIAA, Washington, D.C., 1991), Vol. 137, Chap. 5, pp. 265-340.
- ¹⁵J. P. Drummond and P. Givi, "Suppression and enhancement of mixing in high-speed reacting flow fields," in *Combustion in High-Speed Flows*, edited by M. Y. Hussaini, J. D. Buckmaster, T. L. Jackson, and A. Kumar (Kluwer Academic, The Netherlands, 1994).
- ¹⁶C. M. Coats, "Coherent structures in combustion," *Prog. Energy Combust. Sci.* **22**, 427 (1996).
- ¹⁷D. C. Haworth and T. Poinsot, "Numerical simulation of Lewis number effects in turbulent premixed flames," *J. Fluid Mech.* **244**, 405 (1992).
- ¹⁸S. Mahalingam, J. H. Chen, and L. Vervisch, "Finite-rate chemistry and transient effects in direct numerical simulations of turbulent nonpremixed flames," *Combust. Flame* **102**, 285 (1995).
- ¹⁹O. N. Boratav, S. E. Elghobashi, and R. Zhong, "On the alignment of strain vorticity and scalar gradient in turbulent, buoyant, nonpremixed flames," *Phys. Fluids* **10**, 2260 (1998).
- ²⁰A. Q. Eschenroeder, "Intensification of turbulence by chemical heat release," *Phys. Fluids* **7**, 1735 (1964).
- ²¹J. C. Hill, "Homogeneous turbulent mixing with chemical reaction," *Annu. Rev. Fluid Mech.* **8**, 135 (1976).
- ²²R. M. Kerr, "High-order derivative correlations and the alignment of small-scale structures in isotropic numerical turbulence," *J. Fluid Mech.* **153**, 31 (1985).
- ²³V. Eswaran and S. B. Pope, "Direct numerical simulations of the turbulent mixing of a passive scalar," *Phys. Fluids* **31**, 506 (1988).
- ²⁴P. A. McMurtry and P. Givi, "Direct numerical simulations of mixing and reaction in a nonpremixed homogeneous turbulent flow," *Combust. Flame* **77**, 171 (1989).
- ²⁵A. D. Leonard and J. C. Hill, "Mixing and chemical reaction in sheared and nonsheared homogeneous turbulence," *Fluid Dyn. Res.* **10**, 273 (1992).
- ²⁶G. R. Ruetsch and M. R. Maxey, "The evolution of small-scale structures in homogeneous-isotropic turbulence," *Phys. Fluids A* **4**, 2747 (1992).
- ²⁷Jayesh and Z. Warhaft, "Probability distribution, conditional dissipation, and transport of passive temperature fluctuations in grid-generated turbulence," *Phys. Fluids A* **4**, 2292 (1992).
- ²⁸K. K. Nomura and S. E. Elghobashi, "Mixing characteristics of an inhomogeneous scalar in isotropic and homogeneous sheared turbulence," *Phys. Fluids A* **4**, 606 (1992).
- ²⁹R. O. Fox, "The spectral relaxation model of the scalar dissipation rate in homogeneous turbulence," *Phys. Fluids* **7**, 1082 (1995).
- ³⁰R. O. Fox, "The Lagrangian spectral relaxation model of the scalar dissipation in homogeneous turbulence," *Phys. Fluids* **9**, 2364 (1997).
- ³¹M. R. Overholt and S. B. Pope, "Direct numerical simulations of a passive scalar with imposed mean gradient in isotropic turbulence," *Phys. Fluids* **8**, 3128 (1996).
- ³²F. A. Jaberi, R. S. Miller, C. K. Madnia, and P. Givi, "Non-Gaussian scalar statistics in homogeneous turbulence," *J. Fluid Mech.* **313**, 241 (1996).
- ³³F. A. Jaberi, R. S. Miller, F. Mashayek, and P. Givi, "Differential diffusion in binary scalar mixing and reaction," *Combust. Flame* **109**, 561 (1997).
- ³⁴G. A. Blaisdell, N. N. Mansour, and W. C. Reynolds, "Compressibility effects on the growth and structure of homogeneous turbulent shear flow," *J. Fluid Mech.* **256**, 443 (1993).
- ³⁵X. D. Cai, E. E. O'Brien, and F. Ladeinde, "Advection of mass fraction in forced, homogeneous, compressible turbulence," *Phys. Fluids* **10**, 2249 (1998).
- ³⁶G. Balakrishnan, S. Sarkar, and F. A. Williams, "Direct numerical simulation of diffusion flames with large heat release in compressible homogeneous turbulence," *AIAA Paper 95-2375*, 1995.
- ³⁷F. A. Jaberi and C. K. Madnia, "Effects of heat of reaction on homogeneous compressible turbulence," *J. Sci. Comput.* **13**, 201 (1998).
- ³⁸M. P. Martin and G. V. Candler, "Effects of chemical reactions on decaying isotropic turbulence," *Phys. Fluids* **10**, 1715 (1998).
- ³⁹D. Gottlieb and S. A. Orszag, *Numerical Analysis of Spectral Methods: Theory and Applications* (SIAM, Philadelphia, PA, 1977).
- ⁴⁰P. Givi, "Spectral and random vortex methods in turbulent reacting flows," in *Turbulent Reacting Flows*, edited by P. A. Libby and F. A. Williams (Academic, London, 1994), Chap. 8, pp. 475-572.
- ⁴¹G. Erlebacher, M. Y. Hussaini, H. O. Kreiss, and S. Sarkar, "The analysis and simulation of compressible turbulence," *Theor. Comput. Fluid Dyn.* **2**, 73 (1990).
- ⁴²S. Kida and S. A. Orszag, "Energy and spectral dynamics in forced compressible turbulence," *J. Sci. Comput.* **5**, 85 (1990).
- ⁴³S. Ghosh and W. H. Matthaeus, "Low Mach number two-dimensional hydrodynamic turbulence: Energy budget and density fluctuations in polytropic fluid," *Phys. Fluids A* **4**, 148 (1992).
- ⁴⁴S. Kida and S. A. Orszag, "Energy and spectral dynamics in decaying compressible turbulence," *J. Sci. Comput.* **7**, 1 (1991).
- ⁴⁵F. Marble and J. Broadwell, "The coherent flame model of non-premixed turbulent combustion," Technical report, Project Squid TRW-9-PU, Project Squid Headquarters, Chafee Hall, Purdue University, 1977.
- ⁴⁶E. Van Kalmthout and D. Veynante, "Direct numerical simulations analysis of flame surface density models for nonpremixed turbulent combustion," *Phys. Fluids* **10**, 2347 (1998).
- ⁴⁷S. Pope, "The evolution of surfaces in turbulence," *Int. J. Eng. Sci.* **26**, 445 (1988).
- ⁴⁸J. S. Hewett and C. K. Madnia, "Flame-vortex interactions in a reacting vortex ring," *Phys. Fluids* **10**, 189 (1998).
- ⁴⁹C. D. Pierce and P. Moin, "Large eddy simulation of a confined jet combustor with finite-rate chemistry," *Bull. Am. Phys. Soc.* **43**, 2062 (1998).
- ⁵⁰W. T. Ashurst, A. R. Kerstein, R. M. Kerr, and C. H. Gibson, "Alignment of vorticity and scalar gradient with strain rate in simulated Navier-Stokes turbulence," *Phys. Fluids* **30**, 2343 (1987).
- ⁵¹W. T. Ashurst, "Vortex simulation of unsteady wrinkled laminar flames," *Combust. Sci. Technol.* **52**, 325 (1987).
- ⁵²A. D. Leonard and J. C. Hill, "Direct numerical simulation of turbulent flows with chemical reaction," *J. Sci. Comput.* **3**, 25 (1988).
- ⁵³A. Vincent and M. Meneguzzi, "The spatial structure and statistical properties of homogeneous turbulence," *J. Fluid Mech.* **225**, 1 (1991).
- ⁵⁴G. R. Ruetsch and M. R. Maxey, "Small-scale features of vorticity and passive scalar fields in homogeneous-isotropic turbulence," *Phys. Fluids A* **3**, 1587 (1991).
- ⁵⁵R. S. Miller, F. A. Jaberi, C. K. Madnia, and P. Givi, "The structure and

- small-scale intermittency of passive scalars in homogeneous turbulence,” *J. Sci. Comput.* **10**, 151 (1995).
- ⁵⁶Z. S. She, E. Jackson, and S. A. Orszag, “Scale-dependent intermittency and coherence in turbulence,” *J. Sci. Comput.* **3**, 407 (1988).
- ⁵⁷J. Jimenez, A. A. Wray, P. G. Saffman, and R. S. Rogallo, “The structure of intense vorticity in isotropic turbulence,” *J. Fluid Mech.* **255**, 65 (1993).
- ⁵⁸K. K. Nomura and G. K. Post, “The structure and dynamics of vorticity and rate of strain in incompressible homogeneous turbulence,” *J. Fluid Mech.* **377**, 65 (1998).
- ⁵⁹K. Nomura and S. Elgobashi, “The structure of inhomogeneous turbulence in variable density nonpremixed flames,” *Theor. Comput. Fluid Dyn.* **5**, 153 (1993).
- ⁶⁰W. T. Ashurst and P. A. McMurtry, “Flame generation of vorticity: vortex dipoles from monopoles,” *Combust. Sci. Technol.* **66**, 7 (1989).
- ⁶¹W. T. Ashurst, “Flame propagation along a vortex: The baroclinic push,” *Combust. Sci. Technol.* **112**, 175 (1996).
- ⁶²S. Kida and S. A. Orszag, “Enstrophy budget in decaying compressible turbulence,” *J. Sci. Comput.* **5**, 1 (1990).